

Investigation of Low Emission Reverse Flow Combustors

Submitted in partial fulfillment of the requirements
for

Dual Degree

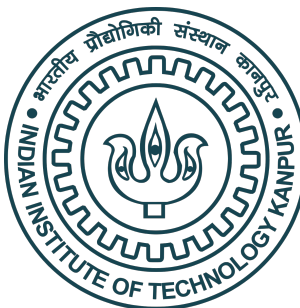
by

Ankit Lakhial

18807102

Under the supervision of

Dr. Vaibhav Arghode, Dr. Kaushal Nishad



Department of Aerospace Engineering
Indian Institute of Technology Kanpur
Uttar Pradesh, India - 208016
June 2024

CERTIFICATE

This is to certify that the thesis entitled "**Investigation of Low Emission Reverse Flow Combustors**", submitted by **Ankit Lakhial** to Indian Institute of Technology Kanpur, is a record of bonafide research work under my supervision and I consider it worthy of consideration for the Dual Degree of the Institute.

Dr. Vaibhav Arghode

Supervisor

Department of Aerospace Engineering
Indian Institute of Technology Kanpur
Kanpur-208016, India

Dr. Kaushal Nishad

Co-Supervisor

Simulation of reactive Thermo-Fluid System
Institute of Reactive Flows and Diagnostics
TU Darmstadt, Darmstadt-64287, Germany

Place: Indian Institute of Technology Kanpur

Date: November 23, 2024

DECLARATION

This is to certify that the thesis titled **Investigation of Low Emission Reverse Flow Combustors** has been authored by me. It presents the research conducted by me under the supervision of Dr. Vaibhav Arghode, Dr. Kaushal Nishad.

To the best of my knowledge, it is an original work, both in terms of research content and narrative, and has not been submitted elsewhere, in part or in full, for a degree. Further, due credit has been attributed to the relevant state-of-the-art and collaborations (if any) with appropriate citations and acknowledgements, in line with established norms and practices.

Name: Ankit Lakhial
Programme: BT-MT (Dual)
Department: Aerospace Engineering
Indian Institute of Technology Kanpur
Kanpur 208016

ABSTRACT

Combustion of hydrocarbon fuels has been a major source of energy for many industries, including transportation, power generation, and heating. While hydrocarbon fuels are abundant and widely available, their combustion is associated with the emission of pollutants such as CO, NOx, UHC, and soot, which can have detrimental effects on both human health and the environment. Peripheral vortex reverse flow (PVRF) and stagnation point reverse flow (SPRF) combustors have been demonstrated to result in low pollutant emissions and stable combustion. In this study, the performance of a PVRF and an SPRF combustor is experimentally and numerically investigated. Compressed natural gas (CNG) is used as the fuel with combustor heat load of 6.25 kW. The combustor has cuboidal shape with dimensions of 80 mm × 80 mm × 40 mm with air/fuel injection ports as well as the exhaust port located at the top side to facilitate an overall reverse flow geometry. The air/fuel injection ports are located at the center of the top side. In the non-premixed mode, fuel is injected coaxially w.r.t. the air jet, whereas in the premixed mode the fuel is mixed with the air at a far upstream location to allow complete mixing before introducing the mixture into the combustor. Both air and fuel injection velocities are relatively high (30-100 m/s) to generate high turbulence and mixing. The PVRF combustor has a single exhaust on one of the sides of the air/fuel injection port that facilitates a strong peripheral vortex on the other side of the combustor. The SPRF combustor has two exhausts located on either sides of the air/fuel injection ports having gas recirculation from both the sides of the air injection. Experiments were conducted to measure NOx, CO emissions, operational limits and CH* chemiluminescence imaging is done to locate the reaction zone. Simulations were performed using RANS models and global chemical kinetic mechanisms to understand the flow field and gas recirculation pattern inside the combustor. Very low (< 5 ppm NOx at equivalence ratio of 0.6) emission levels were obtained for both SPRF and PVRF combustors in both non-premixed and premixed modes of operation. The trends for NOx and CO w.r.t. the equivalence ratio were also same for both PVRF and SPRF combustors. It was observed that the PVRF combustor resulted in slightly lower NOx emissions in the non-premixed mode as compared to the premixed mode. Numerical simulations suggest higher recirculation ratios for the PVRF combustor and compared to the SPRF combustor. The reaction zone location also varies considerably for premixed and non-premixed modes for both combustors.

Keywords: Peripheral vortex reverse flow, Stagnation point reverse flow, Non-premixed combustion, Premixed combustion, Emissions

Acknowledgement

I would like to express my deepest gratitude to my thesis supervisor Dr. Vaibhav Arhode for his invaluable guidance, support, and mentorship throughout this project. His expertise, insightful feedback, and constant encouragement have been instrumental in shaping my understanding and enhancing the quality of my work. I would also like to extend my heartfelt appreciation to co-supervisor Dr. Kaushal Nishad for his valuable contributions and collaboration. His dedication, knowledge, and enthusiasm have greatly enriched the research process and outcomes. I am immensely grateful to Anil Ji, our lab assistant, for his tireless efforts in facilitating the smooth functioning of the laboratory. His technical assistance and willingness to go above and beyond have been truly commendable. I would also like to acknowledge my lab partners for their camaraderie, cooperation, and teamwork. Their support and collective efforts have made this journey both enjoyable and productive. Lastly, I would like to express my gratitude to my friends who have provided unwavering support, encouragement, and motivation throughout this endeavor. I am truly fortunate to have had the opportunity to work with such exceptional individuals, and their contributions have been invaluable in the successful completion of this project.

Ankit Lakhial

List of Tables

4.1	Numerical model specification	31
4.2	Combustor design and operating parameters.	32
4.3	Emitting species found in a hydrocarbon flame and their characteristic wavelength	35

List of Figures

1.1	Conventional gas turbine combustor.	3
1.2	Pollutant emissions variation with equivalence ratio	5
1.3	Comprehensive NOx formation mechanism	8
1.4	NOx variation with flame temperature for liquid and gaseous fuels	9
1.5	Flow configurations of CDC combustor	15
2.1	Schematic of HiTAC chamber	17
2.2	Experimental setup of CDC	17
2.3	FLOX burner	18
2.4	Schematic of MILD combustion	19
2.5	PAWC configuraiton	20
2.6	Schematic of FODI	20
2.7	Schematic of HILE burner	21
2.8	Schematic of JSR	21
2.9	Schematic of TVC	22
2.10	DLN combustor	23
2.11	Schematic of PVRF combustor	23
2.12	Experimental setup of SPRF combustor	24
3.1	Turbulent mixing time and residence time plots.	28
4.1	Numerical mesh generated for the both combustor (PVRF, SPRF)	30
4.2	PVRF combustor experimental setup schematic	33
4.3	SPRF combustor experimental setup schematic	34
4.4	PVRF combustor schematic and photograph	36
4.5	SPRF combustor schematic and photograph	37
5.1	Velocity Contours.	39
5.2	Temprature contours.	40
5.3	Recirculation Ratio.	41
5.4	Global flame photographs of PVRF & SPRF combustor	43
5.5	CH* chemiluminescence intensity images.	44
5.6	CH* chemiluminescence data.	45
5.7	CO and NOx Emissions.	45
5.8	Nox vs CH* intensity and lean operational limit.	46

List of Notations and Operations

ϕ	Equivalence Ratio	—
\dot{m}_{recirc}	Mass flow rate (reactants + entrained gases)	[Kg/s]
\dot{m}_{inj}	Net mass flow rate of the incoming fresh reactants(fuel+air)	[Kg/s]
MW_i	Molecular weights of the species i	[g/mole]
X_i	Mole fraction of species i	—
P_{inlet}	Inlet pressure of inlet	[Pa]
P_{exit}	Inlet pressure of exit	[Pa]
T_3	Temperature at the combustor inlet	[K]
T_4^{max}	Maximum temperature at the combustor exit	[K]
T_4^{avg}	Average temperature at the combustor exit	[K]
ΔH_{CV}	Lower heating value of the fuel	[MJ/Kg]
EI_i	Emission index of species i	[g/Kg or ppm]
τ_{mix}	Mixing time	[s]
U	Air injection velocity	[m/s]
D	Jet diameter	[mm]
t_{res}	Residence time	[s]

Abbreviations

PVRF	Peripheral Vortex Reverse Flow
SPRF	Stagnation Point Reverse Flow
FLOX	Flameless oxidation
HiTAC	High temperature air combustion
MILD	Moderate Intense and Low oxygen dilution
CDC	Colourless distributed combustion
FODI	Fuel/oxidant direct injection
PAWC	Princeton asymmetric whirl Combustor
JSR	Jet Stirred Reactor
TVC	Trapped Vortex Combustor
DLN	Dry Low NO _x
CNG	Compressed Natural Gas
UHC	Unburned Hydrocarbon
CO	Carbon Monoxide
RANS	Reynolds Averaged Navier-Stokes
SIMPLE	Semi-Implicit Method for Pressure-Linked Equations
EDCM	Eddy dissipation concept model
LOL	Lean Operational Limit

Contents

Acknowledgement	v
List of Tables	vi
List of Figures	vii
List of Symbols	vii
List of Abbreviations	ix
1 Introduction	1
1.1 Background	1
1.2 Motivation	2
1.3 Gas Turbine Combustor Design Parameters	2
1.4 Gas Turbine Combustor Design Parameter	4
1.4.1 High Thermal Intensity	4
1.4.2 Low Pollutant Emission	4
1.4.3 Pressure Drop	5
1.4.4 Pattern Factor	6
1.4.5 Combustion Efficiency	6
1.4.6 Combustion Instability	6
1.4.7 Operational Limit	7
1.5 Pollutant Formation	7
1.5.1 Oxides of Nitrogen (NOx)	7
1.5.2 CO (UHC) formation	13
1.5.3 Soot Formation	13
1.6 Nomenclature for different flow configurations	14
2 Literature Review	16
2.1 Introduction	16
2.2 High Temperature Air Combustion (HiTAC)	16
2.3 Colorless Distributed Combustion (CDC)	17
2.4 Flameless Oxidation (FLOX)	18
2.5 Moderate Intense and Low oxygen Dilution (MILD)	19
2.6 Princeton Asymmetric Whirl Combustor (PAWC)	20
2.7 Fuel/oxidant direct injection (FODI)	20
2.8 High Intensity Low Emission Burner (HILE)	21
2.9 Jet Stirred Reactor (JSR)	21
2.10 Trapped Vortex Combustor (TVC)	22
2.11 Dry Low NOx (DLN)	23
2.12 Peripheral Vortex Reverse Flow (PVRF)	23

CONTENTS

2.13 Stagnation Point Reverse Flow (SPRF)	24
2.14 Objectives	25
3 CDC Design Parameters	26
3.1 Introduction	26
3.2 Fuel/Oxidizer Mixing	26
3.3 Gas Recirculation	27
3.4 Thermal Intensity & Residence Time	28
4 Numerical and Experimental Methodologies	29
4.1 Introduction	29
4.2 Numerical setup	29
4.2.1 Combustor Mesh	29
4.2.2 Initial and Boundary Conditions	30
4.2.3 Turbulence and Combustion Model	30
4.3 Experimental Setup	32
4.3.1 Global Imaging	33
4.3.2 CH* Chemiluminescence	34
4.3.3 Gas Analyzer	35
4.3.4 Combustor Design and Ignition Process	35
5 Results and Discussion	38
5.1 Numerical results	38
5.1.1 Flow field Characteristics	38
5.1.2 Temperature field characteristics	40
5.1.3 Recirculation ratio	40
5.2 Experimental Results	42
5.2.1 Global Imaging	42
5.2.2 CH* chemiluminescence	42
5.2.3 Emissions characteristics	43
6 Conclusions and Future Scope	47
6.1 Conclusions	47
6.2 Future scope	47
References	49

CHAPTER 1

Introduction

1.1 Background

Lean combustion is utilized across various sectors of combustion technologies, including boilers, internal combustion engines, furnaces, and gas turbines. The broad application range aims to capitalize under fuel lean conditions on the benefits of operating combustion processes, which offer both high efficiency and low emissions. By maintaining low flame temperatures, pollutant emissions are effectively reduced, particularly in terms of thermal nitric oxide formation. Furthermore, when lean conditions are achieved with excess air during hydrocarbon combustion, complete fuel burnout is typically achieved, resulting in decreased emissions of hydrocarbons and carbon monoxide. However, implementing these enhancements and meeting the practical requirements of combustion systems is challenging due to factors such as slow reaction rates, the possibility of extinction, sensitivity to mixing, instability, and mild heat release.

Emerging technology of Colourless Distributed Combustion (CDC) [1, 2] has the potential to meet the stringent demands for reduced pollution and improved reliability in upcoming gas turbine technologies. Low emission of nitrogen oxides (NOx) is a crucial characteristic of gas turbine engines. Concentrated release of aircraft emissions in specific regions and the lower stratosphere intensifies the impact of the aviation industry's relatively small contribution to overall emissions. Land-based gas turbine engines contribute significantly to NOx and CO emissions, alongside aviation-related gas turbine engines. High demand for power generation engines can be attributed to their lower capital investment costs, superior thermodynamic efficiencies, and current affordability of natural gas. Increasing stringency of environmental regulations concerning NOx emissions for gas turbines and other power generation technologies is a consequential factor that accompanies the growth of gas turbine engines. Implementation of regulations have led to a drive for continuous and extensive research on novel gas turbine combustor technologies, which can

1.2 Motivation

effectively mitigate NOx emissions. Potential of colourless distributed combustor to meet power requirements similar to conventional combustors, while also addressing relevant environmental regulations, is a promising development.

In the present study, reverse flow configuration of CDC combustor have been discussed. In this configuration, inlet and outlet are on same side of the combustor. Reverse flow nature of the geometry allows the product gases to recirculate within the combustion chamber and mix with the incoming oxidizer stream and hence diluting it. This drives the combustion towards colorless regime.

1.2 Motivation

Concerns about the effects of pollutants on the environment and health have led to a heightened focus on pollutant emissions. Over the past decades, there have been significant changes in both regulations and technologies aimed at controlling emissions from gas turbines. Additionally, stationary gas turbines have gained prominence in the gas and oil industry, expanding their applications in combined cycle plants and utility power generation. As a result, there is more demand on combustion engineers to reduce pollutant emissions from different kinds of gas turbines [3].

NOx is a concerning pollutant among other pollutants due to its harmful impact on health and contribution to ozone layer depletion. With the growing demand for land-based and aviation gas turbines, there is an urgent need to minimize gas turbine engines emissions. Several factors, particularly NOx, have a crucial role in the development of pollutants. Formation of nitrogen oxides (NOx) is primarily influenced by the flame temperature and the duration of combustion products in the chamber. Zeldovich mechanism [4], additionally referred to as the thermal NOx mechanism, is one of the various mechanisms for NOx generation and is of utmost significance [5]. Similar to the NOx produced in just a few milliseconds as the temperature near 2100 K [6], thermal NOx is produced at roughly 1800 K over a period of time.

Design and development of a novel combustor which can change the dynamics of combustion process to suppress NOx emission will be explored in next chapter.

1.3 Gas Turbine Combustor Design Parameters

There are wide range of basic requirements that a gas turbine needs to satisfy. The geometry of the combustor is determined by certain key factors. Figure 1.1 illustrate a conventional gas turbine combustor highlighting the geometrical aspects of widely used combustion chamber. There could be multiple variations on this fundamental pattern, however, in general, combustion chamber have

1.3 Gas Turbine Combustor Design Parameters

diffuser, air casing, fuel injector and liner as basic components.

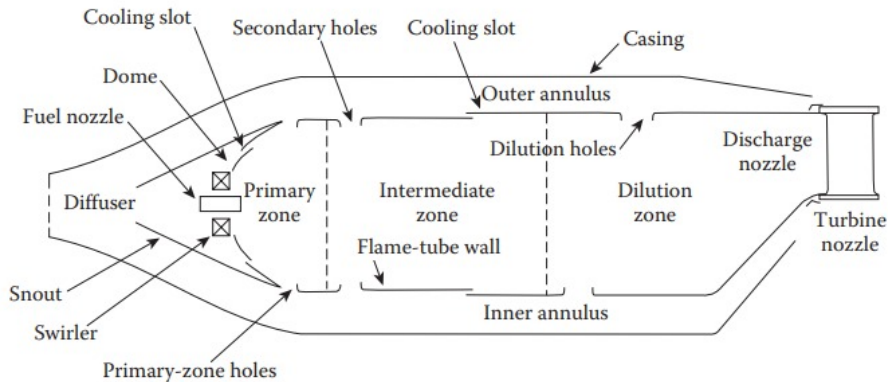


Figure 1.1: Conventional gas turbine combustor [4]

In order to reduce the pressure drop in the combustor, a diffuser is typically used to slow the air as it enters the combustion chamber. Swirlers help to stabilise flames by creating a recirculating flow field in the primary zone. To keep gas temperature within safe range for the turbine blades as it moves downstream from the primary zone, air is injected through liner holes. Temperature profile of the exhaust gases entering the turbine vanes can be modified thanks to this air injection [5].

The fundamental requirements for most combustors [5] are outlined as follows:

- **High combustion efficiency:** The combustion chamber should facilitate complete burning of the injected fuel, ensuring that its entire chemical energy is converted into heat.
- **Wide stability limits:** The combustor needs to operate reliably across a broad range of conditions, including varying pressures and air/fuel ratios.
- **Reliable and smooth ignition:** Aircraft engines must be capable of smooth ignition both on the ground, particularly in cold weather, and at high altitudes where air density is significantly reduced after a flameout.
- **Low pressure loss:** Acceptable pressure loss typically falls within the range of 4-8%.
- **Uniform temperature profile at the outlet (pattern factor):** Lifespan of turbine blades can be maximized by uniform distribution of temperature at the outlet.
- **Low emissions:** The gas turbine engines should comply with the pollution control regulations set by international authorities, ensuring minimal pollutant emissions.
- **Free from combustion instabilities:** Combustion instabilities should be minimized to prevent damage to the combustor hardware and ensure stable operation.

1.4 Gas Turbine Combustor Design Parameter

- **Compact size:** Combustor design must meet the shape and size requirements of gas turbine engines.
- **Fuel flexibility:** Combustor should be capable of accommodating various fuel types, typically kerosene-based for aircraft gas turbines.
- **Ease of maintenance:** Combustor's geometry should allow for convenient maintenance in the event of any reported issues.

1.4 Gas Turbine Combustor Design Parameter

1.4.1 High Thermal Intensity

Thermal intensity refers to the heat energy released rate per unit volume of the combustor, scaled by the operating pressure [1]. In land based gas turbine combustor, typically exhibits a thermal intensity of approximately 5-15 MW/m³-atm.

$$\text{Thermal intensity} = \frac{\text{Heat release rate}}{\text{Volume} \times \text{Pressure}} \quad (1.1)$$

Consequently, high thermal intensity results in high thermal load within a small combustor volume. This is crucial for aerospace applications as it enables space and weight savings in the engine design.

1.4.2 Low Pollutant Emission

Primary pollutants released from the gas turbine combustor include NOx, CO, UHC, and soot. NOx emissions tend to be higher at higher equivalence ratios, reaching a peak at stoichiometric conditions, and decrease in fuel-rich conditions. Conversely, high levels of CO and UHC emissions are observed at both high and low equivalence ratios [7]. Therefore, there exists a limited range where both NOx and CO emissions remain low and within acceptable limits, as depicted in Figure 1.2. Soot, composed of unburnt carbon particles, is primarily generated under fuel-rich conditions.

Level of pollution released by a combustor can be quantified using Emission Index. Emission Index is defined in various ways, such as in grams per kilogram (g/kg) or parts per million by volume (ppm) at a specified O₂ concentration.

$$\text{Emission index}_i = \frac{\text{Mass flow rate of emitted species (g)}}{\text{Mass flow rate of fuel (kg)}} \quad (1.2)$$

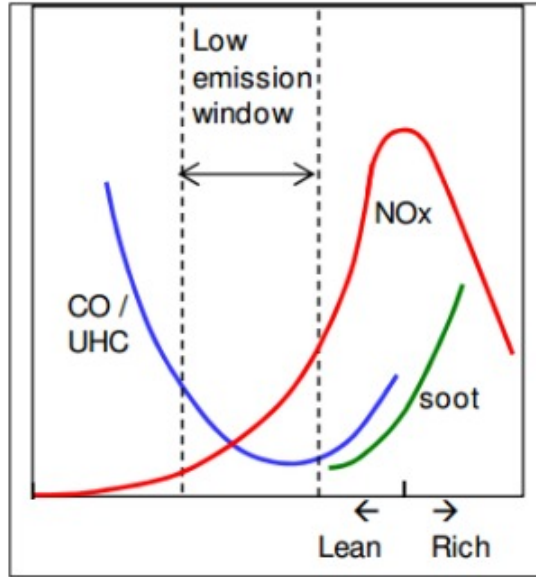


Figure 1.2: Pollutant emissions variation with equivalence ratio [8].

This index represents the amount of pollutant generated per unit mass of fuel. In the case of hydrocarbon fuels, Emission Index is determined based on the mole fraction of species containing carbon.

$$\text{Emission index}_i = \frac{X_i}{X_{CO} + X_{CO_2} + x * X_{UHC}} \frac{(x+2)MW_i}{MW_f} \quad (1.3)$$

Where

$$X^s = \frac{X_i}{X_{CO} + X_{CO_2} + x * X_{UHC}}$$

are mole fractions, MW_i and MW_f are the molecular weights of the species i and the fuel [9], respectively and x is the number of moles of carbon in a mole of fuel, [10].

1.4.3 Pressure Drop

The major cause of pressure losses within a combustion chamber is primarily attributed to the increase in temperature resulting from the combustion process. Additionally, pressure losses can occur due to cold losses caused by friction and inherent pressure losses. In the context of a gas turbine combustor, it is essential to minimize pressure drop since it directly affects the loss of thrust generated by the engine.

$$\text{Pressure drop} = \frac{P_{inlet} - P_{exit}}{P_{inlet}} \quad (1.4)$$

Total pressure at the inlet and exit of the combustor is represented by P_{inlet} and P_{exit} , respectively. Typically, the total pressure drop ranges from approximately 4% to 7% of the inlet total

1.4 Gas Turbine Combustor Design Parameter

pressure for aircraft engines, while for land-based gas-turbine combustors, it is around 1% to 2% [11].

1.4.4 Pattern Factor

Pattern factor, also known as Temperature Traverse Quality, quantifies the non-uniformity of temperature at the turbine inlet (or combustor exit) and is normalized based on the average temperature difference between the exit and inlet. When designing the gas turbine combustion chamber, it is crucial to achieve a suitable and consistent temperature distribution at the turbine exit. The pattern factor directly impacts the engine's power output and the longevity and robustness of the turbine blades located downstream of the combustor.

$$\text{Pattern factor} = \frac{T_4^{\max} - T_4^{\text{avg}}}{T_4^{\text{avg}} - T_3} \quad (1.5)$$

In the equation, T_4^{\max} denotes the highest temperature achieved at the combustor exit, T_4^{avg} represents the average temperature across the combustor exit, and T_3 corresponds to the temperature at the combustor inlet. A pattern factor that approaches zero indicates an ideal scenario with highly uniform temperatures across the combustor exit. Conversely, a pattern factor exceeding 0.4 suggests a non-uniform temperature distribution, which is considered undesirable [12].

1.4.5 Combustion Efficiency

The combustion efficiency is a metric that indicates the effectiveness of utilizing the fuel in the combustion process. Coembustion efficiency is defined as [11]:

$$\text{Combustion efficiency} = \frac{100}{\Delta H_{CV}} [\Delta H_{CV} - ((\Delta H_{CV} \times EI_{CO}) + (EI_{UHC} \times \Delta H_{CV}))] \quad (1.6)$$

Where EI_{CO} is the emission index of carbon monoxide, EI_{UHC} is the emission index of unburned hydrocarbons, ΔH_{CV} is the lower heating value of the fuel.

1.4.6 Combustion Instability

Combustion instabilities arise from significant pressure oscillations caused by the interaction between natural acoustic mode and the oscillatory heat release process of the combustor. These oscillations can escalate from small disturbances to sustained limit cycle oscillations. Combustion instabilities become more pronounced close to the lean operational limit of modern ultra-lean premixed or partially premixed combustors. It is crucial to mitigate these instabilities during com-

1.5 Pollutant Formation

bustion to prevent fatigue, thermal stress on combustor components, and potential complete failure of the combustor over time.

1.4.7 Operational Limit

The operational limits of a combustion chamber are determined by the minimum and maximum equivalence ratio required to sustain a flame. The lean operational limit refers to the minimum equivalence ratio at which the flame remains stable without blowing off. Conversely, the rich operational limit represents the maximum equivalence ratio at which the flame can be sustained before extinguishing. The actual equivalence ratio within the combustion chamber varies due to mixing effects. A larger difference between lean and rich operational limits indicates greater combustion stability, highlighting the importance of achieving a wider range for enhanced stability in the combustion process.

1.5 Pollutant Formation

One of the most crucial factors to consider is the emission of pollutants from the combustor. It is essential to minimize these emissions due to the stricter aircraft emission standards worldwide. Primary pollutants released from the gas turbine combustor include NOx, CO, UHC, and soot. NOx emissions tend to be higher near stoichiometric stoichiometric conditions, and decrease in fuel-rich conditions. Conversely, higher CO and UHC emissions are measured at both low and high equivalence ratios [1]. Consequently, there is only a limited range where both CO and NOx emissions are low and within acceptable limits, as illustrated in Figure 1.2. Soot comprises unburnt carbon particles and is primarily generated under fuel-rich conditions.

1.5.1 Oxides of Nitrogen (NOx)

Majority of nitric oxide (NO) generated during combustion undergoes oxidation to form nitrogen dioxide (NO₂). Due to this, it is common practice to combine NO and NO₂ and refer to them collectively as NOx, instead of solely focusing on NO. NOx can be formed in four different mechanism: thermal NOx, prompt NOx, nitrous oxide mechanism, and fuel NOx.

Thermal NOx Formation (Zeldovich Mechanism)

Thermal NOx formation is a prominent mechanism by which nitrogen oxides (NOx) are generated during combustion processes. Understanding this intricate mechanism is vital for developing effective strategies to mitigate NOx emissions and reduce their environmental impact. The following

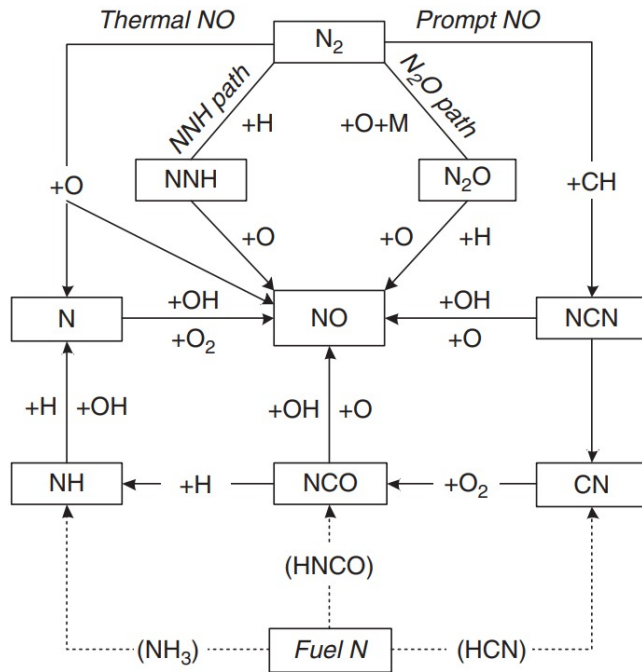


Figure 1.3: Comprehensive NOx formation mechanism [4].

steps help to understand the complex process of thermal NOx formation mechanism:

Nitrogen Fixation: The thermal NOx formation mechanism begins with the thermal dissociation of atmospheric nitrogen (N_2) into individual nitrogen atoms (N^*). This dissociation occurs when high temperatures, typically in excess of 1850 K, are reached during combustion. The energy from the combustion process breaks the strong bonds holding the N_2 molecules together, resulting in the release of highly reactive nitrogen atoms.

Nitric Oxide Formation: Once the nitrogen atoms (N^*) are generated, they react with oxygen molecules (O_2) to form nitric oxide (NO) through a series of intermediate reactions.

The key steps involved in the development of nitric oxide include:

- $\text{N}_2 + \text{O}_2 \rightarrow 2\text{NO}$: The formation of nitric oxide (NO) is mainly driven by the high temperatures reached during combustion. Nitrogen (N_2) from the air reacts with oxygen (O_2) to produce nitric oxide. This reaction is highly exothermic and occurs rapidly.
- $\text{N} + \text{O}_2 \rightarrow \text{NO} + \text{O}$: The nitrogen atom (N) reacts with another oxygen molecule (O_2) to produce additional an oxygen atom (O) and nitric oxide (NO). This reaction contributes to the overall formation of nitric oxide.

Nitrogen Dioxide Formation: Once nitric oxide (NO) is formed, it can further react with oxygen to produce nitrogen dioxide (NO_2), which is a significant component of NOx emissions.

Formation of nitrogen dioxide involves the following steps:

1.5 Pollutant Formation

- $2\text{NO} + \text{O}_2 \longleftrightarrow 2\text{NO}_2$: Nitric oxide (NO) reacts with an oxygen molecule (O_2) to generate nitrogen dioxide (NO_2). This reaction is relatively slow compared to the development of nitric oxide.
- $\text{NO}_2 \longleftrightarrow \text{NO} + \text{O}$: Nitrogen dioxide (NO_2) can also dissociate back into nitric oxide (NO) and an oxygen atom (O) through a reversible reaction. This equilibrium reaction plays a important role in the combustion system to determining the overall concentration of NO_2 .

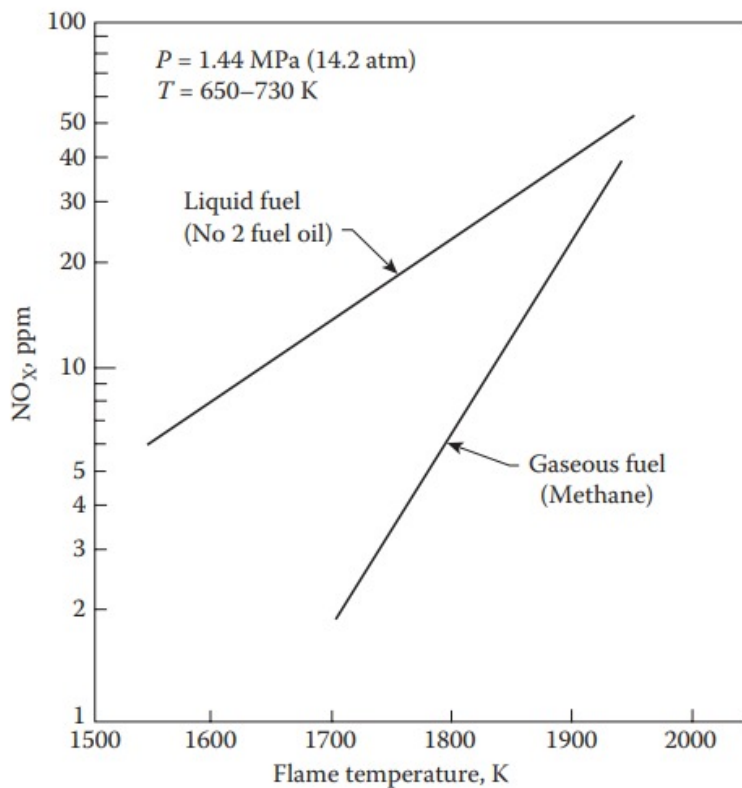
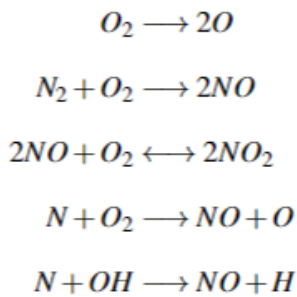


Figure 1.4: NO_x variation with flame temperature for liquid and gaseous fuels [13].

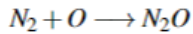
Impact of Operating Conditions on Thermal NO_x Formation: Several factors influence the extent of thermal NO_x formation during combustion processes. Key factors include:

1.5 Pollutant Formation

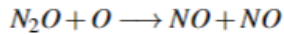
- Temperature: Thermal NOx formation rate increases exponentially with temperature. A high combustion temperature leads to a higher concentration of nitrogen atoms (N^*) and, consequently, increased NOx formation, see Figure 1.4.
- Oxygen Concentration: Availability of oxygen affects the reactions involving nitrogen atoms and nitric oxide. Insufficient oxygen can lead to the accumulation of nitrogen atoms and a subsequent increase in NOx formation.
- Residence Time: The duration that reactant molecules spend within the high-temperature combustion zone, known as the residence time, impacts the overall NOx formation. Longer residence times allow for more extensive nitrogen-oxygen reactions, leading to increased NOx emissions.
- Fuel Composition: Nitrogen-containing compounds in fuels (coal or certain liquid fuels) contribute to the overall NOx formation during combustion.

Nitrous Oxide Mechanism

The following step is initiate the reaction



and formed nitrous oxide (N_2O) is then oxidized to NO by the following reaction [3].



Prompt NOx Formation

Prompt NOx production contributes significantly to NOx emissions in combustion processes, particularly in fuel-rich situations. The following process highlight the prompt NOx mechanism:

Fuel-Rich Combustion Conditions: Prompt NOx formation occurs primarily in fuel-rich environments, such as those encountered in certain types of combustion systems like engines and gas turbines. In these conditions, availability of fuel is relatively high compared to the available oxygen for combustion, leading to incomplete oxidation of the fuel.

Nitrogen Radical Generation: During fuel-rich combustion, high temperatures break down nitrogen-containing species in the fuel, such as nitrogen compounds or fuel-bound nitrogen, releasing nitrogen radicals (N^*) into the combustion zone.

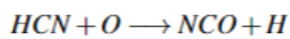
1.5 Pollutant Formation

Key steps involved in nitrogen radical generation include:

- Fuel Decomposition: High temperatures cause the fuel molecules to decompose, releasing reactive hydrocarbon radicals and nitrogen-containing radicals.
- Thermal Dissociation: Nitrogen-containing species undergo thermal dissociation, leading to the formation of highly reactive nitrogen radicals (N^*).

Hydrocarbon Radical Reactions: In fuel-rich conditions, hydrocarbon radicals present in the combustion zone can react with nitrogen radicals to form prompt NOx species. These reactions contribute to the overall prompt NOx formation. The key pathways of hydrocarbon radical reactions include:

- Hydrocarbon-Nitrogen Radical Reaction: Hydrocarbon radicals react with nitrogen radicals (N^*) to form prompt NOx species, such as nitroalkanes and alkyl nitrates. Exact reactions involved depend on the specific hydrocarbon radicals and nitrogen radicals present.



The extent of prompt NOx formation is influenced by various operating conditions and factors:

- Fuel-Richness: The degree of fuel-richness in the combustion environment significantly affects prompt NOx formation. Higher fuel-to-air ratios result in more significant prompt NOx emissions.
- Residence Time: The residence time, or the duration that the reactant molecules spend within the fuel-rich zone, impacts the overall prompt NOx formation. Longer residence times allow for more extensive hydrocarbon-nitrogen radical reactions, leading to increased prompt NOx emissions.
- Temperature: Although prompt NOx formation is more prominent in fuel-rich conditions, high temperatures still play a role. Increased temperatures enhance the decomposition of nitrogen-containing species and facilitate the generation of nitrogen radicals for reactions with hydrocarbon radicals.

1.5 Pollutant Formation

Fuel NOx Formation

Fuel-bound nitrogen oxides (fuel NOx) play a significant role in the formation of NOx emissions during combustion processes. The following process highlight the fuel NOx mechanism:

Nitrogen Compounds in Fuel: Many fuels, including coal, oil, and biomass, contain varying amounts of nitrogen compounds. These compounds can be categorized into two main groups: organic nitrogen compounds and inorganic nitrogen compounds. Organic nitrogen compounds are derived from biomaterials and fossil fuels, while inorganic nitrogen compounds include ammonia and nitrates.

Nitrogen Release during Combustion: When fuel is subjected to high temperatures during combustion, the nitrogen compounds present undergo thermal decomposition, releasing nitrogen species into the combustion zone. The nitrogen species then participate in various reactions, leading to the formation of fuel NOx.

The key pathways of fuel NOx formation include:

- **Nitrogen Oxide Formation:** Organic nitrogen compounds decompose, releasing nitrogen radicals (N^*) into the combustion zone. These nitrogen radicals rapidly react with oxygen molecules (O_2) to form nitric oxide (NO). The released nitrogen oxide can further react to form nitrogen dioxide (NO_2), which contributes to the overall fuel NOx emissions.
- **Nitrogen-Atom Transfer:** Inorganic nitrogen compounds, such as ammonia (NH_3), decompose into nitrogen atoms (N^*). These nitrogen atoms reaction with oxygen or other reactive species in combustion chamber, can lead to form nitric oxide (NO). This process is known as nitrogen-atom transfer and is a significant contributor to fuel NOx emissions.
- **Nitrous Oxide Formation:** Some fuel nitrogen compounds, particularly nitrogen-based heterocyclic compounds found in coal and biomass, can also contribute to the formation of nitrous oxide (N_2O) during combustion. Nitrous oxide is a potent greenhouse gas and a minor contributor to fuel NOx emissions.

The extent of fuel NOx formation is influenced by several fuel-related factors:

- **Fuel Nitrogen Content:** The nitrogen content of the fuel plays a crucial role in determining the potential for fuel NOx formation. Fuels with higher nitrogen content have a higher propensity to generate fuel NOx emissions.
- **Fuel Composition:** Different fuel types contain varying organic and inorganic nitrogen compounds, leading to differences in the fuel NOx formation potential. For example, coal gener-

1.5 Pollutant Formation

ally contains higher nitrogen content compared to natural gas, resulting in higher fuel NO_x emissions when combusted.

- **Fuel Processing:** Fuel processing techniques, such as desulfurization and denitrification, can reduce the amount of nitrogen in the fuel and subsequently lower the fuel NO_x formation potential.

1.5.2 CO (UHC) formation

It typically emerges when the combustion zone operates in a fuel-rich state, where there isn't enough oxygen for complete conversion to CO₂. CO is produced significantly even under stoichiometric conditions or slightly fuel-lean conditions due to the dissociation of CO₂. In lean conditions, characterized by a slow burning rate, CO levels tend to be high because of the slower conversion of CO to CO₂, where the time spent in the combustion process is a crucial factor. It has been observed that there is a correlation between CO and UHC emissions, as the factors influencing CO also affect UHC [5].

1.5.3 Soot Formation

Soot formation occurs through a complex series of chemical reactions during the combustion process. The key steps involved in the formation of soot particles are:

- **Fuel Pyrolysis:** When fuel is exposed to high temperatures in the presence of limited oxygen, it undergoes pyrolysis, breaking down into smaller hydrocarbon fragments.
- **Nucleation:** In regions of fuel-rich environments, small carbonaceous particles begin to form through nucleation. These particles are primarily composed of polycyclic aromatic hydrocarbons (PAHs) and other carbon-rich species.
- **Surface Growth:** The nucleated particles grow by absorbing other hydrocarbons present in the combustion environment. The growth occurs through the deposition of additional carbon onto the existing particles, resulting in larger and more complex structures.
- **Aggregation:** The grown soot particles may aggregate with each other, forming larger agglomerates.
- **Soot Oxidation:** In the presence of oxygen, soot particles can undergo oxidation, which can result in the eventual destruction of the particles. However, in fuel-rich environments with limited oxygen availability, this oxidation process is inhibited, leading to the accumulation of soot.

1.6 Nomenclature for different flow configurations

Several factors affect the formation of soot in combustors, including:

- **Fuel Composition:** The chemical composition of the fuel significantly influences soot formation. Fuels with higher carbon content, such as heavy oils or coal, are more prone to soot formation compared to cleaner fuels like natural gas or hydrogen.
- **Air-Fuel Ratio:** The air-fuel ratio plays a crucial role in soot formation. Fuel-rich conditions, where there is an insufficient supply of oxygen for complete combustion, promote soot formation. Insufficient oxygen limits the availability of oxidants needed for complete combustion and encourages the formation of carbonaceous particles.
- **Residence Time:** The residence time, or the duration that fuel spends in the combustor, also impacts soot formation. Longer residence times provide more opportunities for incomplete combustion and subsequent soot formation.
- **Temperature:** The temperature profile within the combustor affects soot formation. High temperatures can enhance the pyrolysis process, leading to increased soot precursor formation. Additionally, inadequate mixing of fuel and air can result in localized regions of lower temperatures that favor soot formation.

1.6 Nomenclature for different flow configurations

Figure 1.5 shows different flow configurations of CDC combustor, where A represents air port, B represents exit port and F indicate fuel port. In chapter 2, different flow configuration are discussed for various combustion technologies. In the present study also, we will discuss reverse flow configuration for premixed and non-premixed cases.

1.6 Nomenclature for different flow configurations

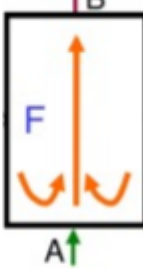
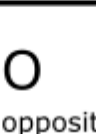
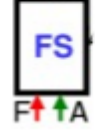
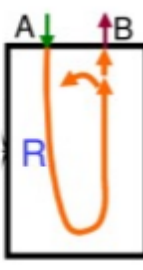
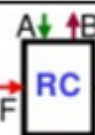
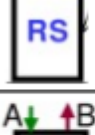
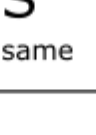
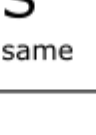
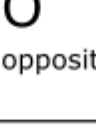
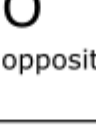
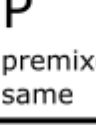
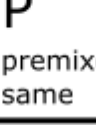
Configurations		Air & Exit Port side (First term)	Air & Fuel Port side (Second term)
Forward flow		 F opposite	 O opposite
		 F opposite	 S same
		 F opposite	 P premixed same
Reverse flow		 R same	 C cross
		 R same	 S same
		 R same	 O opposite
		 R same	 P premixed same

Figure 1.5: Flow configurations of CDC combustor [1].

CHAPTER 2

Literature Review

2.1 Introduction

Low emission combustion techniques such as High Temperature Air Combustion (HiTAC) [14–24], Flameless Oxidation (FLOX) [25–29], Moderate and Intense Low Oxygen Dilution (MILD) combustion [30–36], Colorless Distributed Combustion (CDC) [1, 2, 37–42], Fuel/Oxidant Direct Injection (FODI) furnace [43, 44], Princeton Asymmetric Whirl Combustor (PAWC) [45, 46], High Intensity Low Emission Burner (HILE) [47], Jet Stirred Reactor (JSR) [48] and Trapped Vortex Combustor (TVC) [49], Dry Low NO_x (DLN) [50], Peripheral Vortex Reverse Flow (PVRF) combustor [51–54] and Stagnation Point Reverse Flow (SPRF) combustor [55–59] is discussed.

2.2 High Temperature Air Combustion (HiTAC)

The novel approach involves heating the reactant air to a significantly high temperature, surpassing that of traditional recuperative combustion. This is achieved by exchanging enthalpy between the furnace section's exhaust gases and the fresh incoming air, facilitating heat and mass transfer [16]. Surprisingly, the occurrence of chemical reactions is not dependent on catalysts or reaction promoters in this novel combustion process. The temperature achieved is frequently higher than the fuel-air mixture's auto-ignition temperature, which varies according to the fuel used. This method, known as High Temperature Air Combustion (HiTAC) [15], contrasts with conventional preheated air combustion, which primarily aims to increase the flame temperature. HiTAC flames have stable combustion without the need for a flame stabilizer such as a swirler or bluffbody, resulting in a low pressure drop over the combustor [1].

2.3 Colorless Distributed Combustion (CDC)

An investigation was conducted in [14] to analyze the impact on fuel mixing conditions by varying fuel injector locations. Preheated air was supplied through a square duct with dimensions of $100 \text{ mm} \times 100 \text{ mm}$. The combustion chamber had a length of 300 mm and underwent contraction and expansion to create a recirculating flow. The study involved heating air to a temperature of 1423 K using an alternating-flow regenerative preheater. Figure 2.1 shows fuel injector locations where CNG was used as fuel. The results showed significant variations in NO (nitric oxide) emissions among the different cases. The lowest NO emissions were observed when fuel was injected at location "F3," which resulted in uniform fuel mixing and suggested distributed combustion. It was found that NO emissions in this case were independent of temperature and equivalence ratio. On the other hand, injecting fuel at location "F2" led to very high NO emissions.

2.3 Colorless Distributed Combustion (CDC)

The term "colorless" refers to the flame's low visible emission when compared to conventional flames [37]. The distributed reaction zone facilitates the distributed combustion, which occurs throughout the entire combustion zone. To achieve reactions similar to those of colorless distributed combustion (CDC), certain conditions must be met. These include separating the air and fuel streams to prevent direct reactions and controlling the product gases entrainment in the air stream to create a high-temperature and low-oxygen oxidizer [37]. This oxidizer is then mixed with the fuel jet, leading to spontaneous ignition and creating a distributed combustion reaction zone throughout the entire combustion chamber [37].

The study conducted in [39] investigates CDC and examines the impact of different thermal intensities. The research focuses on thermal intensities ranging from 5 to 453 MW/m³ atm [60],

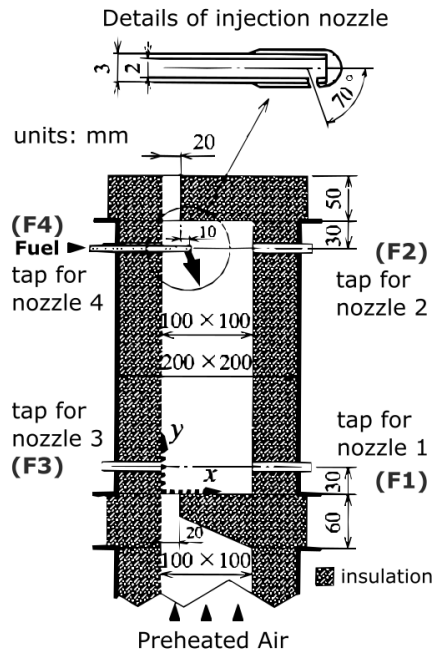


Figure 2.1: Schematic of HiTAC chamber [14].

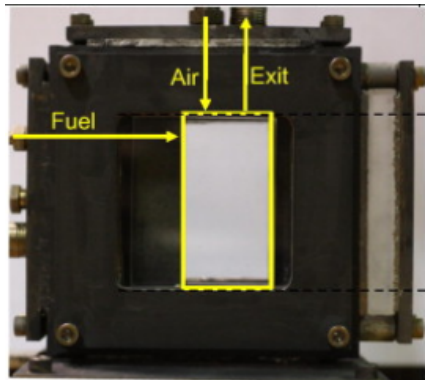


Figure 2.2: Experimental setup of CDC [38].

2.4 Flameless Oxidation (FLOX)

aiming to achieve improved performance without substantial increase in hardware cost. The study explores various flow field configurations and finds that the reverse cross-flow configuration with increased air injection diameter, shown in Figure 2.2, is particularly favorable. At a thermal intensity of 53 MW/m³ atm [60], this configuration achieves low emissions of 4 ppm for NOx and 27 ppm for CO. Further reductions in volume lead to higher thermal intensities and emissions, indicating the potential for significantly increasing thermal intensity while maintaining low emissions.

2.4 Flameless Oxidation (FLOX)

In 1997, the term "flameless oxidation" (FLOX) was introduced in [26] to reduce thermal NOx emissions in the furnace by avoiding hot spots. FLOX involves combustion without a visible or audible flame, achieved through internal gas recirculation. It was noted that air preheat with higher temperatures were used in this study, but air preheat is not always necessary for flameless oxidation. Additionally, flameless mode can be achieved by injecting air and fuel in a direct or discrete way as well as in premixed mode.

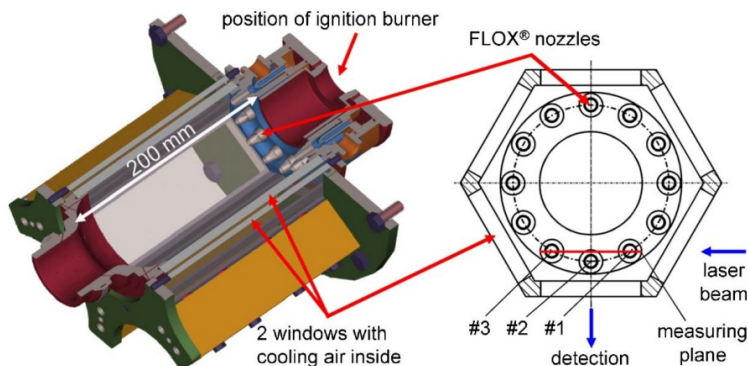


Figure 2.3: FLOX burner [29]

An enhanced FLOX® burner (see Fig. 2.3) was developed and studied in [29] to meet the operational requirements of a gas turbine combustor. Compressed natural gas (CNG) and CNG + hydrogen combustion was experimentally and numerically investigated for relevant conditions of gas turbine. Under specific conditions, such as an inlet velocity of 160 m/s and air preheat temperatures of 700 K, low NOx emissions of 10 ppm were achieved with relatively homogeneous flame zones distributed over a large volume. A stable low-emission operating range was achieved for natural gas and high jet exit velocities. The power densities achieved were 13.3 MW/m³-bar for CNG and 14.8 MW/m³-bar for CNG + H₂, meeting the requirements of a gas turbine combustor. The study shows complete and stable combustion with very low pollutant emissions.

2.5 Moderate Intense and Low oxygen Dilution (MILD)

The term "MILD combustion" as discussed in [30] denotes a combustion process distinguished by specific conditions of reactant temperature and temperature increase. In MILD combustion, the reactants' inlet temperature is higher than the mixture's autoignition temperature, however autoignition temperature of the reactant mixture is always higher than temperature increase during the combustion process [61].

MILD combustion and HiTAC combustion were distinguished based on their respective temperature characteristics. In HiTAC combustion, the temperature rise during the combustion process surpasses reactant's autoignition temperature, despite the reactant temperature being higher than the auto-ignition temperature of the reactant mixture [53]. This differentiation highlights that in HiTAC combustion, the temperature increase exceeds the threshold for self-ignition, while MILD combustion maintains a temperature rise below the auto-ignition point.

The stability characteristics of MILD combustion burner operating in a reverse flow configuration were investigated in [31]. The burner had exhaust at centerline of combustion chamber and it is surrounded by four air injection ports at a distance of 55 mm and four fuel injection ports at a distance of 110 mm (see Fig. 2.4). The study considered various factors such as air preheat temperature, heat extraction, equivalence ratio, and fuel dilution. The baseline case exhibited NOx emissions of approximately 14 ppm. The reduction of the air preheat temperature from 723 K to 300 K led to lower NOx emissions of around 12 ppm. Increasing the amount of heat extraction from 25% to 42% led to a significant decrease in NOx emissions, lowering them from 14 ppm to 7 ppm. Surprisingly, as the equivalence ratio increased from 0.8 to 0.9, it resulted in a reduction in NOx emissions from 14 ppm to 8 ppm. Lower NOx emissions were also reported by diluting fuel with CO₂ or N₂. CO formation is found to be influenced by mixing patterns and furnace temperature rather than

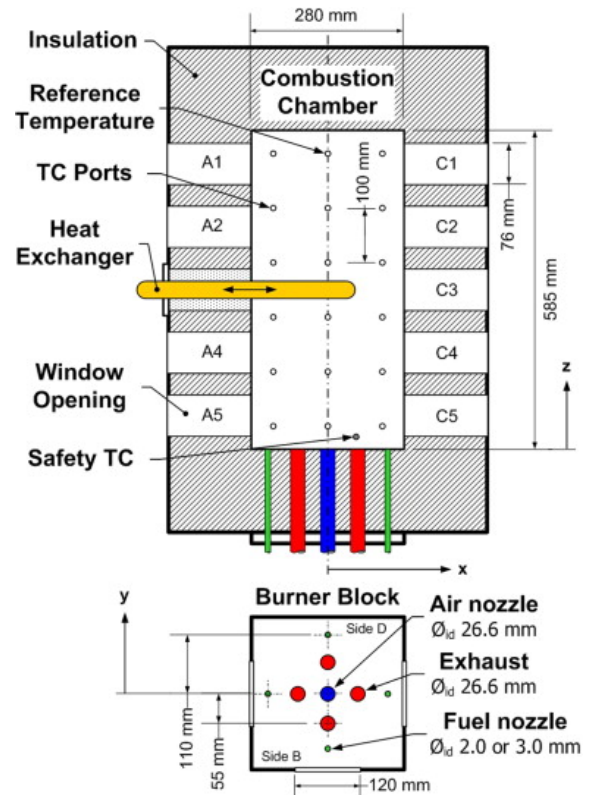


Figure 2.4: Schematic of MILD combustion [31].

2.6 Princeton Asymmetric Whirl Combustor (PAWC)

heat exchanger effects. The study determines the critical equivalence ratio for low CO emissions, identifies an optimum operating condition, and establishes the significance of fuel jet momentum for system stability. Combustion in MILD regime can be achieved by keeping fuel/air momentum ratio around 0.006 with minimum fuel jet momentum.

2.6 Princeton Asymmetric Whirl Combustor (PAWC)

A new and promising method for designing low-NO_x, non-premixed combustors is introduced in [46], where fuel is injected in an off-axis or asymmetric manner into a swirling flame. Experimental investigations using this approach were conducted on a laboratory-scale burner, reacting methane and air under atmospheric conditions. The results showed remarkably low NO emissions, measuring below 15 ppm, accompanied by modest CO emissions below 25 ppm at 15% O₂ [46]. The combustor displayed remarkable stability characteristics, even at overall equivalence ratios as low as 0.1 [46].

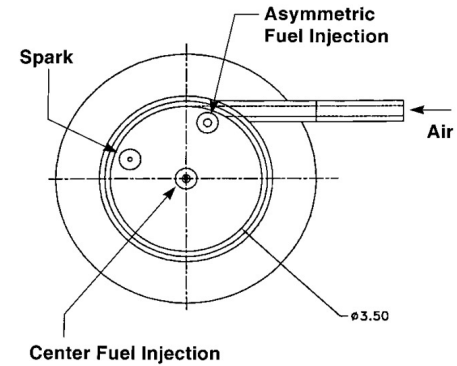


Figure 2.5: PAWC configuraiton [46].

2.7 Fuel/oxidant direct injection (FODI)

A study on strong-Jet/weak-Jet configuration was conducted in [43], where air and fuel injected through a single port (see Fig. 2.6). The air jet with higher momentum was referred to as the “strong jet”, while the fuel jet was called the “weak jet” [1]. The term “Fuel/oxidant direct injection (FODI)” was called due to direct injection of air and fuel into the chamber [1]. The combustor operated at 0.1 MW/m³-atm thermal intensity with reverse flow configuration and were able achieve low CO and NO_x emissions of 34 ppm and 3 ppm, respectively. The study examined the effects of fuel/air nozzle separation, fuel/air momentum flux, and fuel injection angle in depth [1]. Lower injection angles were found to result in reduced NO_x emissions, while higher fuel injection velocities led to greater fuel dilution before combustion, resulting in lower NO_x emissions.

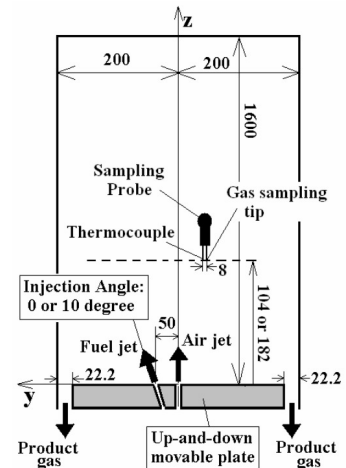


Figure 2.6: Schematic of FODI (units in mm) [43].

2.8 High Intensity Low Emission Burner (HILE)

A study conducted on a HILE, combustor specifically designed for high thermal intensity furnace applications in [47]. Unlike previous studies, which demonstrated thermal intensities below 1 MW/m³-atm, this combustor achieved a thermal intensity of 10 MW/m³-atm. Combustion chamber consists a frustum of cone (see Fig. 2.7) to enhance gas recirculation and achieve a notable reduction of 10-15 dB in noise levels. The study showed that to achieve low emissions, high air preheat temperature was not necessary. Recuperator/regenerator system (used in previous studies) was eliminated just by using air and fuel at ambient temperature as peripheral high-speed jets at the bottom. Although low NO_x emissions of approximately 4 ppm were achieved, the combustor exhibited high levels of CO emissions (2300 ppm), even after the use of staged air with a 10% excess to oxidize CO.

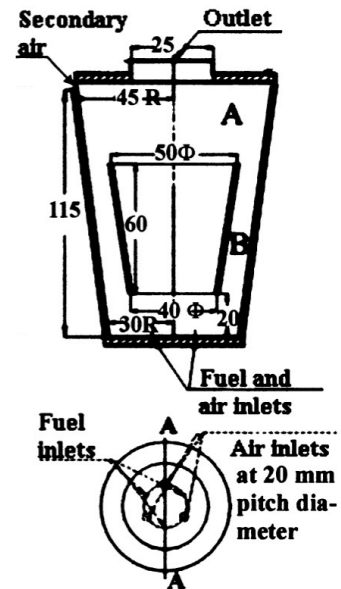


Figure 2.7: Schematic of HILE burner [47].

2.9 Jet Stirred Reactor (JSR)

A JSR in [48], investigated the formation of NOx, operating with lean-premixed methane/air (see Fig. 2.8). The study analyzed the effects of pressure, residence time, and inlet temperature on NOx formation [48]. The results showed that lower residence times resulted in lower NOx levels, while higher concentrations were observed at extreme residence times. Increasing pressure and inlet temperature had a reducing effect on NOx concentrations. Concentration profiles within the reactor indicated two distinct regions: a postflame region and a highly CO concentrated non-equilibrium reaction zone. NOx formation mainly occurred in the non-equilibrium reaction zone. The study also identified a chemical rate-limiting and high-intensity combustion regimes based on the Damköhler number and the ratio of turbulent intensity to laminar burning velocity [48].

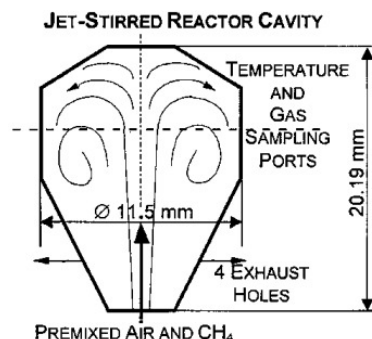


Figure 2.8: Schematic of JSR [48].

2.10 Trapped Vortex Combustor (TVC)

TVC technology in [49] utilizes a unique approach to enhance flame stability by injecting fuel into a confined vortex located between two plates or within a cavity along the combustion airflow path (see Fig. 2.9). This design enables the formation of a concentrated burning reaction zone within the small cavity, resulting in exceptional lean operational limits with an overall equivalence ratio below 0.2. The trapped vortex acts as a continuous ignition source for combustion, as the mixture within it is typically rich [48], generating highly reactive hot gases that readily ignite the mixture in the main combustion chamber. The TVC exhibits a low lean blowout (LBO) limit across a broad operating range due to the shielding of the cavity from the annular air. Without primary air, the length of the cavity strongly influences the LBO limit, with an optimal length of 0.6 times the diameter of the Forebody. Residence time and mixing directly affects the LBO limit in the presence of primary air. Lower LBO limits are achieved at lower primary air flow rates, while higher primary air flows result in a linear increase in the fuel flow rate at the LBO limit. Additionally, the TV-combustor demonstrates a low-pressure drop, offering potential reductions in specific fuel consumption. At a low annular air velocity of 14 m/s, combustion efficiencies were around 99%, decreasing to 97% at a higher velocity of 42 m/s, and reaching 99% with the inclusion of a second cavity. At higher annular air flows, combustion showed a narrower high-efficiency range due to its sensitivity to the primary air. The primary zone is believed to be the primary source of NOx formation.

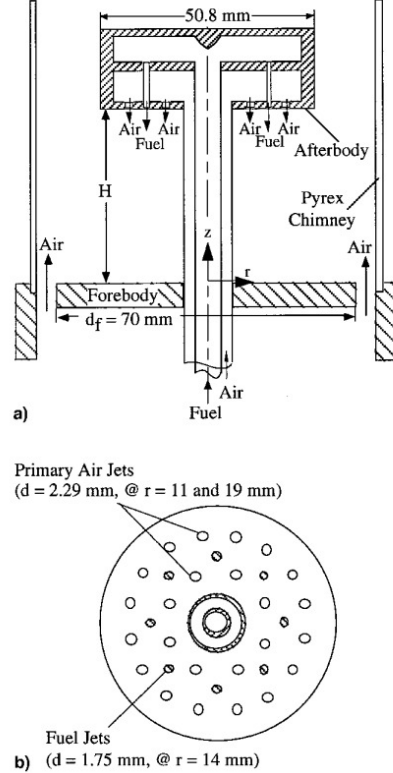


Figure 2.9: Schematic of TVC [49].

2.11 Dry Low NOx (DLN)

2.11 Dry Low NOx (DLN)

The core principle of this combustor is to generate a well-mixed combination of lean air and fuel prior to its introduction into the combustion chamber of a gas turbine. Flame temperature remains relatively low by maintaining lean mixture, resulting in decreased NOx emissions [8].

A DLN combustor investigated in [50] operates at 15MW/m³-atm thermal intensity and a length scale of 1.52 m (see Fig. 2.10). It achieves low emissions, with NOx and CO levels below 9 ppm for load conditions ranging from 50% to 100%. Operating at an inlet temperature of 631K, outlet temperature of 1561K, and an operating pressure of 16 atm, it is applied in GE-7FA gas turbine combustors. The DLN combustion method utilizes lean premixed combustion and fuel staging to effectively reduce NOx emissions across various load conditions.

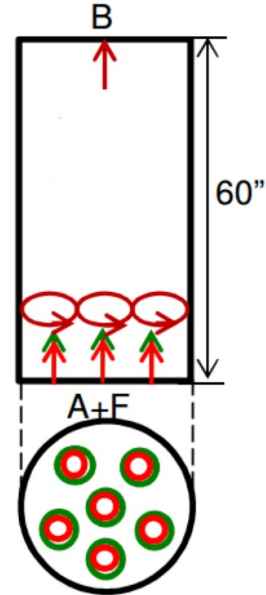


Figure 2.10: DLN combustor [8].

2.12 Peripheral Vortex Reverse Flow (PVRF)

PVRF combustor operates using a reverse flow design. In this combustor, air injects along the center line of the combustor and when the air jet reaches the bottom of the combustor, it splits into two streams, creating two recirculation zones on either side of the air jet due to the reversal of flow [51]. The recirculation zone located near the sidewall and away from the combustor exit in figure 2.11 is referred to as the “peripheral vortex” [51]. This peripheral vortex plays a crucial role in entraining the hot product gases and contributing to the stabilization of reactions.

The PVRF combustor in [52] is examined with a maximum 6.25 kW heat load and 25 MW/m³-atm thermal intensity using ethylene and LPG fuels in both non-premixed and premixed case. Different fuel injection diameters are tested. In the premixed case, maximum NOx emissions of up to 15 ppm and 26 ppm were observed for LPG and ethylene fuels, respectively, at an equivalence ratio of 0.8. Surprisingly, premixed mode reported higher NOx emissions (for both fuels) than non-premixed case. When using LPG fuel, CO emissions were around 100 ppm and 200 ppm for non-premixed

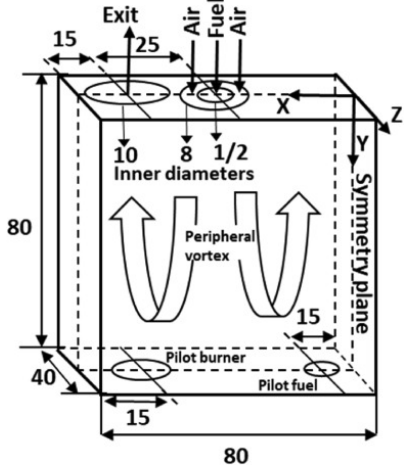


Figure 2.11: Schematic of PVRF combustor [52].

2.13 Stagnation Point Reverse Flow (SPRF)

premixed case, respectively. However, with ethylene fuel, the premixed case showed higher CO emissions than the non-premixed case.

2.13 Stagnation Point Reverse Flow (SPRF)

SPRF is a type of low-emission combustor that features a reverse flow configuration. In this technique, along the center line of the combustor, the reactants are injected coaxially. Upon injection, the reactant jet impinges on the combustor's bottom wall, creating a stagnation zone. This zone splits the reactant jet into two symmetrical streams, resulting in a high turbulence and low velocity region known as the "stagnation point" [56]. Additionally, the combustor design promotes internal recirculation of the hot product gases due to the reverse flow configuration. This unique geometry contributes to the low emissions characteristic of the SPRF combustor.

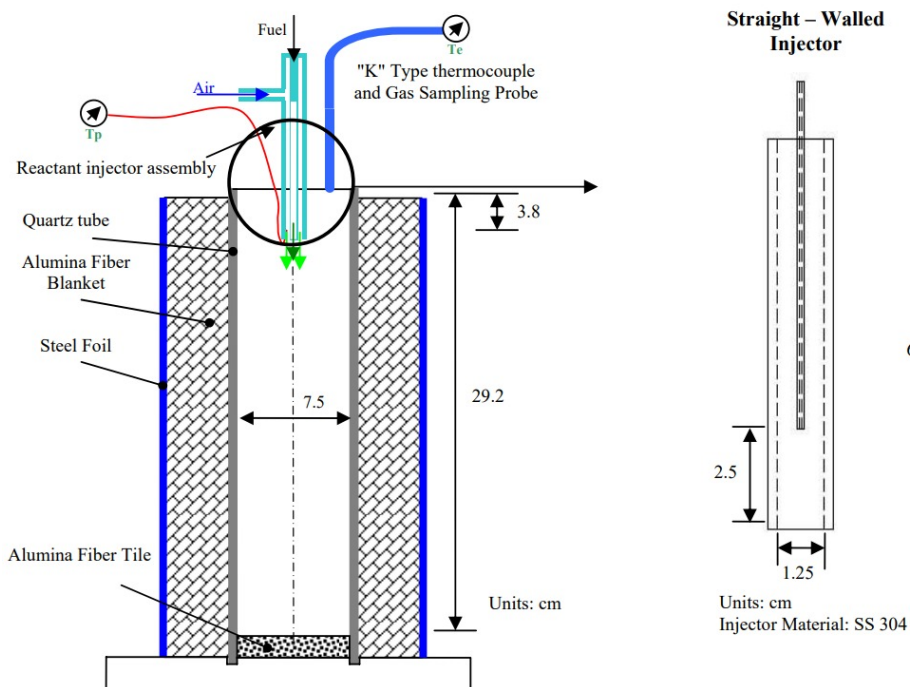


Figure 2.12: Experimental setup of SPRF combustor [57].

SPRF combustor investigated in [57] using an airblast fuel injector to assess the performance of the combustor using Jet-A and heptane liquid fuels. This air blaster was designed for lower mass flux during experiments (see Fig. 2.12). Pressure lossess were kept below 5% using a diffuser. Jet-A fuel showed a stable combustion at heat intensity of 10 MW/m³-atm. Lower NOx emissions (below 1 ppm) and CO emissions (5 ppm) were reported [6].

2.14 Objectives

The current thesis deals with the numerical and experimental investigation of a reverse flow configuration for PVRF and SPRF combustor with the following objectives:

1. To simulate flow field, temperature field characteristics and gas recirculation of air/fuel mixing.
2. To measure the pollutant emissions for a range of equivalence ratios.
3. To investigate reaction zone positioning using CH* chemiluminescence imaging and direct flame photography.
4. Compare the results for both PVRF and SPRF combustor.

CHAPTER 3

CDC Design Parameters

3.1 Introduction

CDC combustor design parameters are discussed in this chapter. The factors are as given below:

- Fuel/oxidizer mixing and ignition delay
- Gas recirculation
- Thermal intensity and residence time
- Flow configurations

While air and fuel direct injection at high momentum are the unique features of colorless combustion technologies, this helps stabilize the flame without any external flame stabilizing mechanism. The effects of the parameters on the efficiency of the combustor are discussed in detail.

3.2 Fuel/Oxidizer Mixing

The calculation of turbulent mixing time depends on the relationship given in equation 3.1 [62,63].

$$\text{Mixing time} = \tau_{mix} = \frac{l_o}{v'_{ms}} = \frac{D}{U} \quad (3.1)$$

where

U : air injection velocity, D : jet diameter

l_o : integral length scale = $\frac{D}{10}$, v'_{ms} : $\frac{U}{10}$ (assuming turbulence intensity = 10%)

This correlation suggests that the turbulent mixing time depends inversely on air injection velocity (U), i.e., ($\tau_{mix} \propto \frac{1}{U}$) and directly on the diameter (D), i.e., ($\tau_{mix} \propto D$) for the same mass flow

3.3 Gas Recirculation

rate. Therefore, increasing injected velocity of air and reducing the diameter of the air injection can lead to a decrease in the mixing time, resulting in a faster mixing of fuel with the oxidizer (see Fig. 3.1a). An increase in diameter results in a longer mixing time, which can potentially lead to insufficient mixing. When mixing is inadequate, it can result in higher pollutant emissions [1].

3.3 Gas Recirculation

In colorless combustion, the entrainment of product gases into fresh reactants is used to increase the temperature of the reactants and decrease the oxygen concentration in the oxidizer. The recirculation ratio determines the extent of gas recirculation by measuring the quantity of product gases entrained into the fresh oxidizer mixture. It is calculated by dividing the mass flux of the recirculated gases by the mass flux of the fresh reactants. A higher equivalence ratio ensures better mixing of fuel and air.

$$\text{Recirculation ratio} = \frac{\text{Entrained product gases mass flow rate}}{\text{Injected air mass flow rate}} \quad (3.2)$$

The correlation given in equation 3.3 below is used to describe the behavior of a non-reacting air jet with variable density when injected into an idle medium [64, 65].

$$\text{Recirculation ratio} = \frac{\dot{m}_{rec}}{\dot{m}_{inj}} = C_e \frac{x}{D^*} - 1 \quad (3.3)$$

where

\dot{m}_{inj}	: initial jet mass flux,	\dot{m}_{rec}	: recirculation mass flux
D^*	: $D(\frac{\rho_{inj}}{\rho_{rec}})^{1/2}$,	C_e	: 0.32
D	: air inject diameter,	x	: distance along the jet centerline
ρ_{inj}	: injected air density,	ρ_{rec}	: recirculated air density

From equation 3.3, following statement can be made:

1. recirculation ratio (RR) directly proportional to distance from the air injection port ($RR \propto x$), i.e. recirculation ratio increases as the distance increases from air injection port upto bottom of the combustor.
2. recirculation ratio is directly dependent upon air injection temperature ($RR \propto T_{air}^{1/2}$).
3. recirculation ratio depends upon injection diameter such that $RR \propto \frac{1}{D}$.

3.4 Thermal Intensity & Residence Time

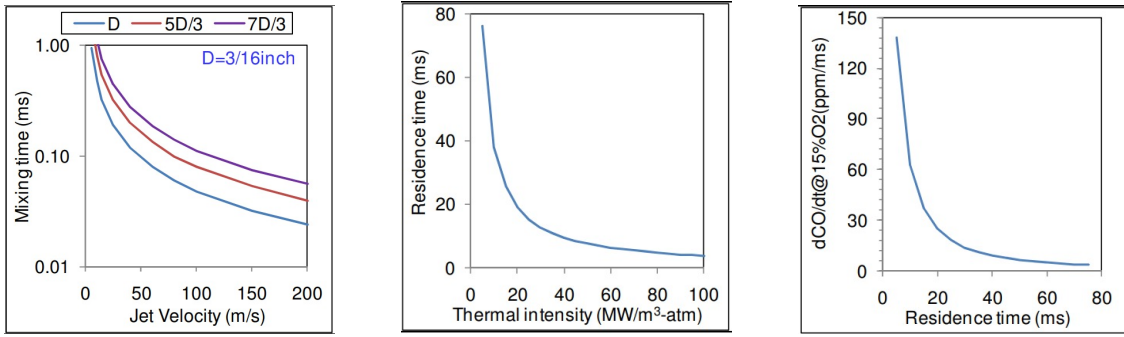
3.4 Thermal Intensity & Residence Time

In Chapter 1, we discussed thermal intensity which is representative of the residence time of gases in the combustor by definition. The residence time depends on thermal intensity inversely in the combustor [1].

$$\text{Residence time} = t_{res} = \frac{\rho V}{\dot{m}} \quad (3.4)$$

where, \dot{m} represents the total mass flow rate through the combustor, ρ is the average gas density in the combustor, and V is the combustor volume.

A higher thermal intensity leads to a shorter residence time (see Fig. 3.1b), which presents various design challenges such as increased velocity and reduced flame stability. Higher CO emissions measured at shorter residence time due to insufficient time for conversion from CO to CO₂, as depicted in figure 3.1c. The graph illustrates that the conversion rate of CO is high at lower residence times.



(a) Turbulent mixing time with variation of diameter and jet velocity [1].

(b) Residence time variation.

(c) conversion rate CO to CO₂.

Figure 3.1: Turbulent mixing time and residence time plots.

CHAPTER 4

Numerical and Experimental Methodologies

4.1 Introduction

The numerical simulations in this study were performed using ANSYS Fluent 2021 R1, a commercially available Computational Fluid Dynamics (CFD) software. The combustor geometry was spatially discretized with structured mesh using ICEM CFD 2021 R1. The main objectives of these simulations were to investigate the flow field, recirculation ratio and the temperature distribution in order to complement the experimental measurement for detailed understating. Both reacting and non-reacting flows were simulated, with a fixed equivalence ratio (ϕ) of 0.8. It is important to note that a consistent 6.25 kW heat load was maintained across all cases. By conducting these numerical simulations under the given operating conditions, a comprehensive understanding of the flow characteristics, temperature profiles, and recirculation patterns can be obtained.

4.2 Numerical setup

4.2.1 Combustor Mesh

In order to simulate the combustor, a three-dimensional geometric model is constructed and meshing is done with using ICEM CFD software. Meshes for both the combustors are shown in figure 4.1. Individual boundaries has been assigned names such as "AIR INLET" and "FUEL INLET" for inlets, "EXIT" for exhaust, "AIR WALL", "FUEL TUBE" and "EXIT WALL" for walls and "SYMM" is assigned to symmetry plane. Only half of the flow domain is discretized into computational domain to reduce the associated computational cost. A total of ≈ 0.7 million hex-hedral

4.2 Numerical setup

structured mesh is created. At circular cross-sections “C-Grid” is created to improve the mesh orthogonality with minimum global quality index of 68% and maximum aspect ratio of ≈ 63 .

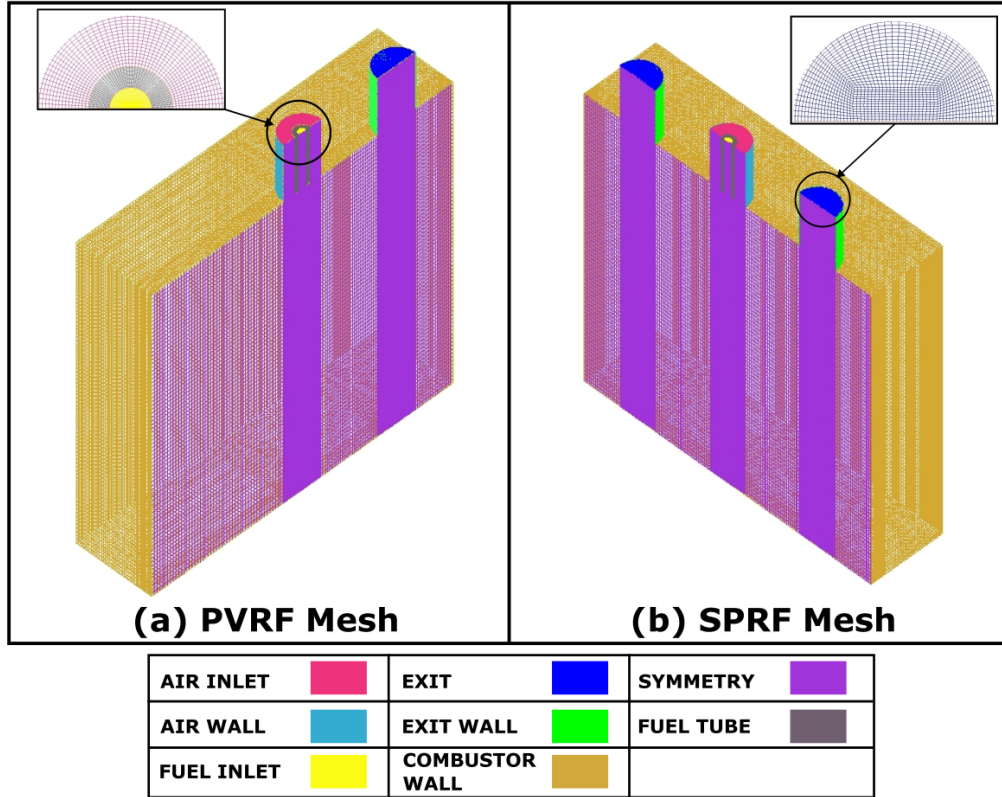


Figure 4.1: Numerical mesh generated for the both combustor (PVRF, SPRF)

4.2.2 Initial and Boundary Conditions

The mass flow inlet boundary condition with air mass flow rate (\dot{m}_{air}) 2.68 g/s and fuel mass flow rate (\dot{m}_{fuel}) 0.125 g/s with O₂ (0.21) and CH₄ (1) species mole fraction is applied to the air and fuel inlets, respectively. Pressure outlet boundary condition with zero gauge pressure (in Pa) and O₂ (0.21) mole fraction is applied to outlet (exit) of the combustor. For walls, no-slip, stationary wall and standard wall roughness with 0.5 roughness constant, adiabatic, non-catalytic and zero diffusive flux for species boundary conditions are applied. Symmetry boundary condition is applied at symmetry plane along which the combustor is cut into half. The operating pressure is 1 atm for all the cases and the initial temperature at the inlet and outlet is 300 K.

4.2.3 Turbulence and Combustion Model

SIMPLE (Semi-Implicit Method for Pressure-Linked Equations) scheme is used for coupling between pressure and velocity in the context of finite volume formulation. Second-order upwind schemes are used to discretize momentum and energy equations, while first-order upwind schemes

4.2 Numerical setup

are employed for other scalar quantities. To solve governing equations, a pressure-based solver is used. Gradients within the computational domain are computed using the least square cell-based method. Turbulence intensity of the mean velocity field is set at 5% with associated hydraulic diameter of 10 mm.

The standard k- ε model, along with standard wall functions, is utilized for turbulence modeling. This model, consisting of two transport equations to captures the diffusion of turbulent energy and convection. In particular, the turbulent kinetic energy (k), reflecting the energy within turbulence, and the turbulent dissipation rate (ε), governing the rate at which k dissipates.

The turbulence-chemistry interactions are accounted by using Eddy Dissipation Concept Model (EDCM), along with a two-step global reaction mechanism with volume fraction constant of 2.137 and time scale constant of 0.41. For mixture of reactants, incompressible ideal gas option is used to calculate density, mixing law is used for specific heat (Cp) calculation. Thermal conductivity is set constant 1.72×10^{-5} and mass diffusivity is set 2.88×10^{-5} using constant-dilute approximation.

Table 4.1 provides a concise overview of the numerical model parameters, encompassing the essential specifications and configurations employed in the simulation.

Table 4.1: Numerical model specification

Turbulence model	RANS with standard k- ε
Fuel	Methane
Oxidizer	Air
Turbulence-chemistry interaction	Eddy dissipation concept model (EDCM)
Pressure-velocity coupling	SIMPLE
Gradient	Least square cell based
Convection term discretization	Second order upwind (pressure, momentum and energy) and first order upwind for other scalars
Spatial discretization	≈ 0.7 M hex-hedral Mesh
Walls	Zero diffusive flux, Non catalytic, no slip, stationary, walls-adiabatic, roughness constant = 0.5
Exhaust	Pressure outlet, 1 atm
Operating Pressure	1 atm
Air and fuel inlet temperature	300 K

4.3 Experimental Setup

The experiments were conducted on a reverse flow configuration. The combustor used in the experiments had a cuboidal shape with dimensions of $80 \text{ mm} \times 80 \text{ mm} \times 40 \text{ mm}$, resulting in a volume of 256 cc. Figure 4.2 and 4.3 shows the experimental setup for PVRF and SPRF combustor. The combustor was constructed using quartz material with a thickness of 10 mm, which provided good optical access for detailed diagnostics.

In this study Compressed Natural Gas (CNG) is used as a fuel, which possesses a heating value of 50 MJ/kg. The experiments were performed under atmospheric conditions, with air and fuel inlet temperatures both maintained at 300 K. To enable thorough observation, the test facility employed for the experiments provided complete optical accessibility. Additionally, the enclosed combustion chamber featured ignition ports, as illustrated in Figure 4.4.

During the experiments, the combustor when operated at 0.8 equivalence ratio (ϕ) represents the 6.25 kW heat load. The ϕ varied in the range of 0.8 to 0.5, with an interval of 0.05. It is important to note that the \dot{m}_{air} was maintained constant at 2.68 g/s throughout the experiments. The mass flux of fuel was adjusted between 0.015 g/s and 0.125 g/s to obtain the required equivalence ratio between 0.5 and 0.8.

Table 4.2: Combustor design and operating parameters.

Combustor	Volume	80 mm x 80 mm x 40 mm (256 cc)
	Heat load	6.25 KW (equivalence ratio = 0.8)
	Exit port diameter	10 mm
Air	Inner diameter	10 mm
	Injection velocity	31.86 m/s @ ($\phi = 0.8$)
	Mass flow rate	2.68 g/s @ ($\phi = 0.8$)
Fuel	Inner diameter	2 mm
	Injection velocity	60.65 m/s @ ($\phi = 0.8$)
	Mass flow rate	0.125 g/s @ ($\phi = 0.8$)
	Outer diameter	4 mm
	Lower heating value	50 MJ/kg
	Density	0.656 kg/m ³

Before collecting the experimental data, a settling period of approximately 20 minutes was allocated to the combustor to establish a stable operating condition. This duration ensured that

4.3 Experimental Setup

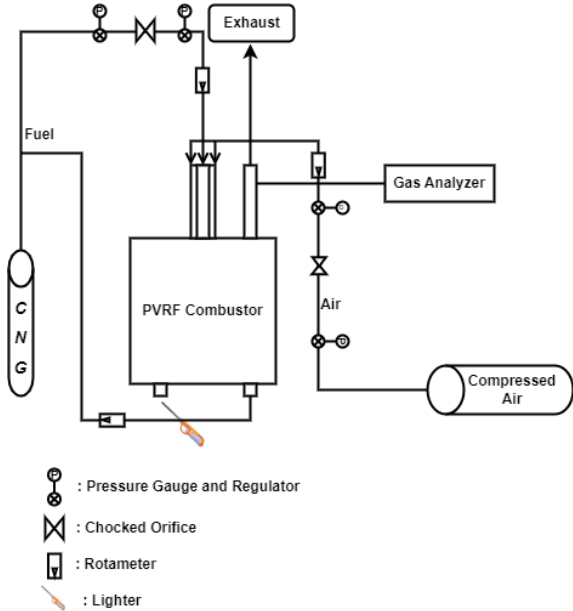


Figure 4.2: PVRF combustor experimental setup schematic

the combustion system reached a fully developed state and maintained consistent performance throughout the subsequent data collection process.

Exhaust gas samples measured by a built-in gas pump was utilized, which drew the gas sample through a probe. The concentration of oxygen in the exhaust gas was measured using a 2-electrode electrochemical sensor based on gas diffusion technology. The pollutant gases emission levels , specifically nitrogen monoxide (NO), and nitrogen dioxide (NO₂) and carbon monoxide (CO), were measured using a 3-electrode sensor consisting of a counter, reference, and sensing electrode.

Whenever experimental conditions were changed, such as adjusting the equivalence ratio, it was ensured that the emission readings would be taken after five minutes. This waiting period was essential to ensure precise measurements by allowing the system ample time to adjust and provide consistent emission data.

In order to address experimental variations, each specific setting or condition was repeated three times during the experiments. An estimated uncertainty of approximately ± 0.5 ppm was associated with the measurement of NOx emissions, while an uncertainty of approximately $\pm 10\%$ was associated with the measurement of CO emissions. These uncertainties reflect the inherent variations in the measurement process and instrumentation.

4.3.1 Global Imaging

The reaction zone of methane-air combustion was captured using a mobile camera with a maximum resolution of 3456×4608 pixels, which corresponds to approximately 15 megapixels. The camera settings used for capturing the images were as follows: a shutter speed of 1/23 s, ISO

4.3 Experimental Setup

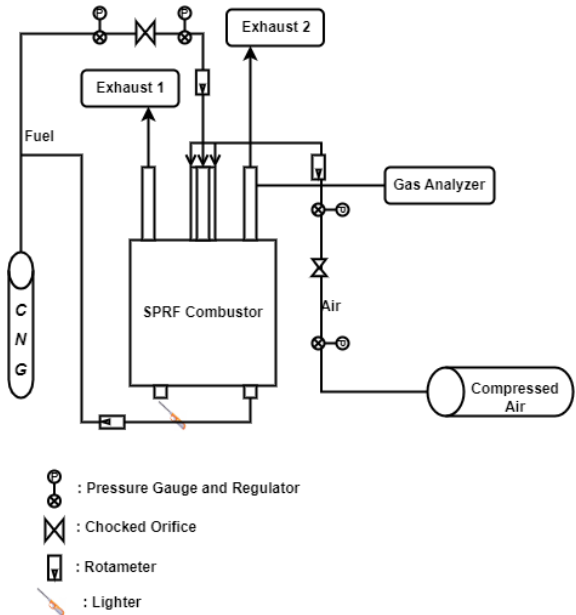


Figure 4.3: SPRF combustor experimental setup schematic

sensitivity set to 100, and an aperture of f/1.8. The camera was positioned at a fixed distance from the combustor for all the images.

It is important to note that images are not post-processed to change the brightness or contrast. The captured images were raw, without any adjustments or enhancements. This ensures that the captured images accurately represent the observed reaction zone without any artificial alterations. By maintaining consistent camera settings and distance from the combustor, the captured images provide a visual representation of the reaction zone for different equivalence ratios in methane-air combustion.

4.3.2 CH* Chemiluminescence

Chemiluminescence is a phenomenon observed in combustion processes where the energy released during a chemical reaction is converted into light. This emission of light occurs when excited molecular electronic states return to their ground state by spontaneously emitting photons [66,67]. The wavelengths of these emitted photons are unique to the species involved in the reaction, and by detecting these wavelengths, valuable information about the presence of specific species in the flame can be obtained.

A selection of commonly observed emitting species in hydrocarbon flames, such as CH^* , C_2^* , OH^* , CO_2^* , and H_2O^* , along with their characteristic wavelengths, is typically provided in Table 4.3. By analyzing the specific wavelengths at which these species emit light, one can identify their presence and gain insights into the combustion processes taking place within the flame.

4.3 Experimental Setup

Emitting Species	Characteristic Wavelength
OH*	308.4 nm
CH*	431.5 nm
C*	436-563 nm
CO_2^*	Broadband from 340-650 nm
Incandescent soot	Continuous (function of temperature)

Table 4.3: Emitting species found in a hydrocarbon flame and their characteristic wavelength (Data is taken from [68]).

4.3.3 Gas Analyzer

In this study, the flue gas analysis was performed using the MRU OPTIMA7 multigas handheld gas analyzer. This analyzer have a built-in gas pump that draw sample of flue gases through a probe from combustor. A built-in filter processed the sample by passing it through condensate separator to ensure it is clean and dry. Finally, electrochemical sensors analyze the gas sample.

The MRU OPTIMA7 gas analyzer is capable of measuring various parameters of the flue gases, such as oxygen (O_2) concentration, carbon monoxide (CO) concentration, nitrogen oxide (NO_x) levels, sulfur dioxide (SO_2) levels, and other relevant combustion gases. The electrochemical sensors in the analyzer provide accurate and real-time measurements of these gas concentrations, allowing for the analysis of flue gas composition and emissions.

4.3.4 Combustor Design and Ignition Process

Figure 4.4 and 4.5 shows schematic and photograph of the PVRF and SPRF combustor. The dimensions of combustor is $80 \times 80 \times 40$ (in mm). The air and fuel injection take place co-axially at the top and along the centerline of the combustor in non-premixed mode. In premixed mode, fuel tube is removed and at far upstream point, air and fuel are mixed properly and then injected in combustion chamber. In the PVRF combustor, the air injection port (with a diameter of 10 mm) is positioned 40 mm from the right wall, while the fuel injection port (with a diameter of 2 mm) is coaxial with the air injection port. The air and exit ports are located at a distance of 25 mm from their respective centres, while the exit port is positioned at a distance of 15 mm from the right wall of the combustor.

In the SPRF combustor, an additional exit port is added at a distance of 25 mm from the air port and 15 mm from the left wall. Both exit ports are symmetrically placed along the air port axis. The ignition port, or pilot burner, is located at the bottom right of the combustor, 15 mm from the

4.3 Experimental Setup

right wall. An external igniter is used to initiate the combustion and is subsequently closed by a insulated plug to avoid any secondary flow. The ignition port has a diameter of 10 mm. The pilot fuel port, used to supply the fuel during initial combustion stage, is situated at the bottom right, 15 mm from the left wall, and has a diameter of 5 mm.

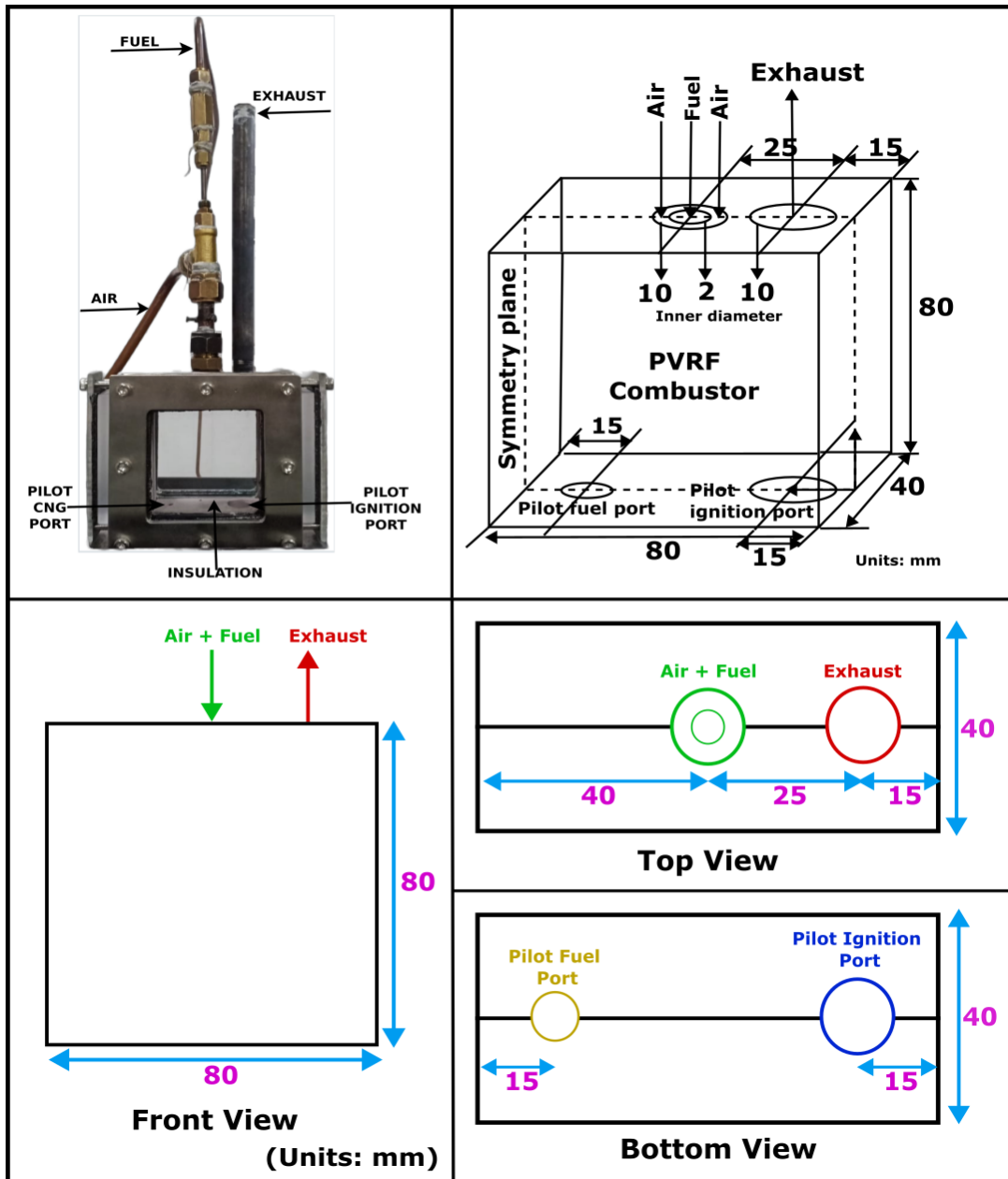


Figure 4.4: PVRF combustor schematic and photograph

4.3 Experimental Setup

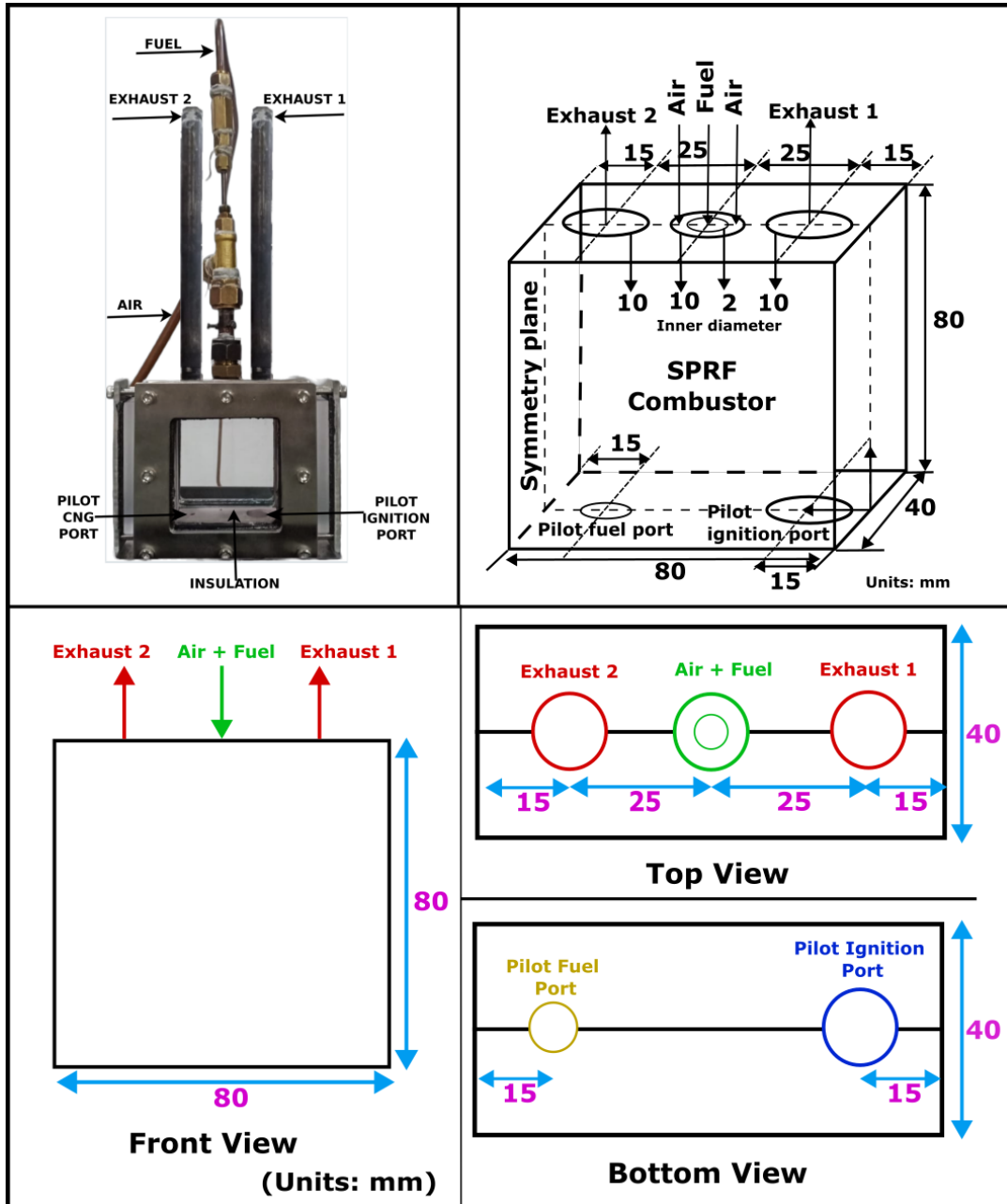


Figure 4.5: SPRF combustor schematic and photograph

CHAPTER 5

Results and Discussion

In this section, numerical and experimental findings will be discussed in detail. The numerical simulations are conducted with a fixed equivalence ratio of $\phi = 0.8$. On the other hand, the experimental results cover a range of equivalence ratios from $\phi = 0.5$ to $\phi = 0.8$. The experimental data includes global images, spatially and temporally averaged CH* data, pollutant emissions, the lean operational limit, and the correlation between emission data and CH* intensity data.

5.1 Numerical results

The steady state numerical simulations are carried out by using commercial softwares ANSYS FLUENT for both the combustor configurations. In particular, both non-reacting and reacting cases were numerically investigated. The obtained numerical results can provides detailed 3-D flow features in terms of the evolution of flow fields, temperature distribution, and recirculation ratios in the combustor.

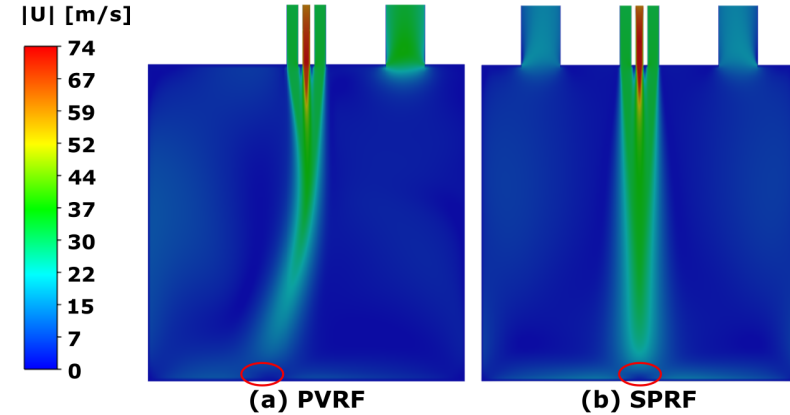
5.1.1 Flow field Characteristics

Non-Reacting case

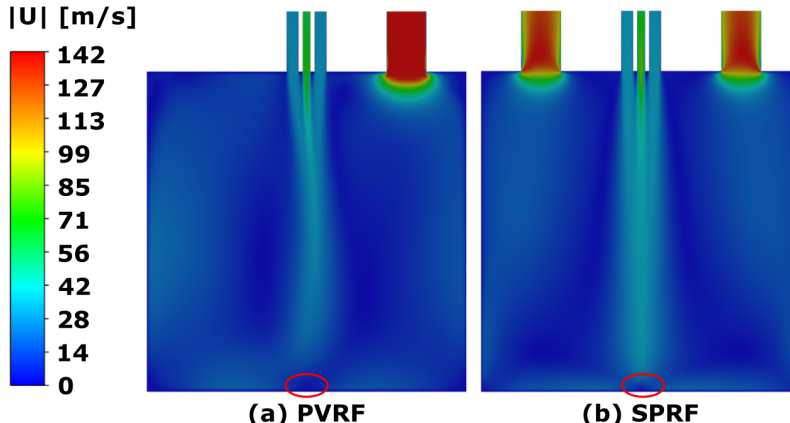
Figure 5.1a shows velocity field for the PVRF and SPRF combustor non-reacting cases. The inlet velocities is 32 m/s for air and 61 m/s for fuel for both the combustors. PVRF combustor shows higher exit velocity around 40 m/s compared to SPRF combustor (i.e., 20 m/s) due to two exit ports in the SPRF combustor. In the SPRF combustor, due to symmetry on both sides of the jet, there is no visible deflection in the jet, while in the PVRF combustor, the jet deflects towards the left wall of the combustor (opposite to the exit port) due to the low pressure region and creates a peripheral vortex. The resultant stagnation points are marked with red circle where its location

5.1 Numerical results

is deviated slightly towards left in the case of PVRF combustor. The visible impact of number of exhaust ports can be clearly seen as the higher velocity is observed in the case of PVRF with single exhaust port.



(a) The mean velocity fields for non-reacting cases



(b) The mean velocity fields for reacting cases

Figure 5.1: Velocity Contours.

Reacting case

Velocity field for the reacting flow is shown in figure 5.1 for both combustors. The air and fuel injection velocity are same as non-reacting cases. There is an overall increase in the velocity magnitude throughout the combustor as compared to the non-reacting cases because of temperature increment and decreased gas density. Again PVRF combustor shows higher exit velocity (240 m/s) than SPRF combustor (120 m/s). The resulting stagnation points for SPRF is still at the centre while, but relatively less deviated in the case of PVRF combustor as compared to non-reacting case. This observation can be attributed to complex flow dynamics and variation of thermo-physical properties of working fluid during combustion process.

5.1 Numerical results

5.1.2 Temperature field characteristics

Figure 5.2 illustrates the temperature contours for both PVRF and SPRF combustors, with the temperature ranging from 300 to 2400 K. The fuel jet is surrounded by the air jet, and at the entry of the reactants, only air is present in the outer boundary of the jet. Due to the considerable recirculation of product gases, the reactions begin further downstream, where the fuel and air mix to form a reactive mixture. In the PVRF combustor, there is a distinct region of relatively lower temperature observed on right sides of the air jet, particularly in the central area of the combustor.

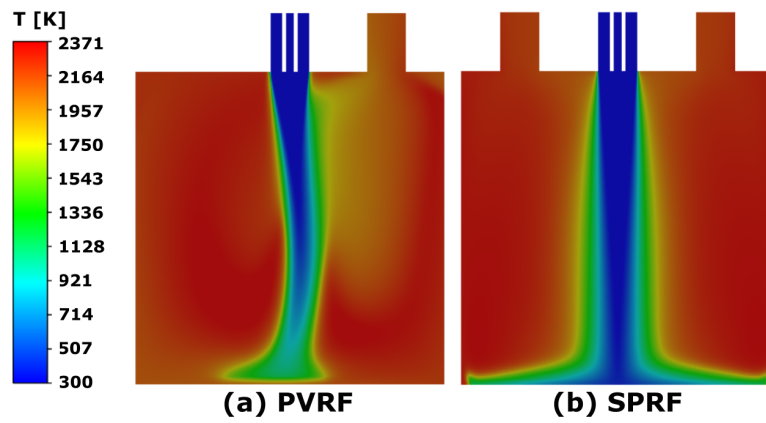


Figure 5.2: Temperature contours.

The rapid mixing facilitates the entrainment of hot flue gases into the reactants. Furthermore, in the SPRF combustor, a relatively more uniform temperature distribution is achieved. This is because of high momentum of the fuel jet and the presence of high-temperature regions surrounding the air jet. As a result, the combustion reaction primarily occurs at the center of the combustor, while the remaining combustion products are evenly distributed throughout the combustor. The bottom section of the combustor exhibits a near-uniform temperature, indicating the presence of a stagnation zone in that region.

5.1.3 Recirculation ratio

Recirculation ratios are calculated for both reacting and non-reacting conditions. To obtain the recirculation ratio, the entrained mass flow rate is divided by the mass flow rate of the injected fresh reactants, which includes both air and fuel.

$$\text{Recirculation Ratio} = \frac{\dot{m}_{recirc} - \dot{m}_{inj}}{\dot{m}_{inj}} \quad (5.1)$$

5.1 Numerical results

Non-Reacting

Figure 5.3a illustrates the evolution of the recirculation ratio of gases within the combustor along the length of the air jet as it progresses. In non-reacting case (see Figure 5.3a), PVRF combustor recirculation ratio increases upto $5 y/D_{air}$ (y is the combustor length in the jet axis) and then starts decreasing. In SPRF combustor recirculation ratio increases upto $4 y/D_{air}$ and then decrease upto $5 y/D_{air}$ then increases again up to $7 y/D_{air}$ then decreases. The recirculation ratio magnitude for SPRF combustor is less than that for PVRF combustor. In both cases, the air jet diminishes as it reaches the bottom of the combustor, but the length of the combustor is not adequate for complete dissipation of the jet. Hence, the mixture reverses back mostly towards the right side as there is a wall present on the left side, which is closer to the jet core. From the right side, the gases rise up towards the exit. These gases tend to move out from the exit, but some gases move towards the incoming reactants. Recirculated gas entrainment increases the recirculation ratio linearly upto $5 y/D_{air}$ and then decreases exponentially due to the presence of a stagnation zone at the lower portion of the combustor. It is important to note that a decrease in the recirculation ratio doesn't imply there is no entrainment rather a weaker flow recirculation .

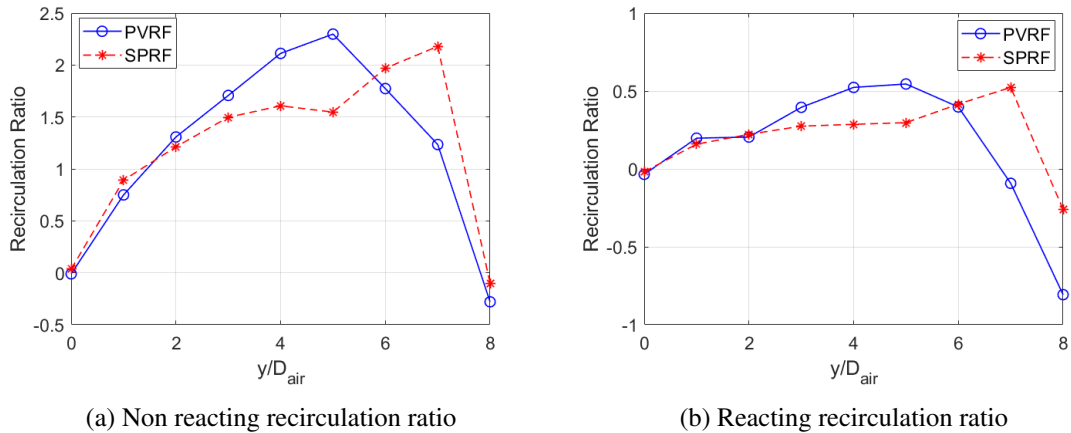


Figure 5.3: Recirculation Ratio.

Reacting

In the case of the reacting flow (refer to Figure 5.3b), the recirculation ratio of the PVRF combustor initially increases until reaching a value of $5 y/D_{air}$, after which it starts to decrease. On the other hand, the recirculation ratio of the SPRF combustor increases until a value of $7 y/D_{air}$ and then decreases. SPRF combustor shows lower recirculation ratio than that of the PVRF combustor. Negative values indicate the existence of a stagnation region. It is noteworthy that the magnitude of the recirculation ratio in the reacting flow case is lower compared to the non-reacting cases.

5.2 Experimental Results

In this section experimental results are discussed. Here CH* chemiluminescence data, global photographs and NOx and CO emissions levels at corrected to 15% O₂, lean operational limit and NOx and CH* intensity relationships are described.

5.2.1 Global Imaging

Global images are used for flame characteristics in the colorless combustion regime. These images, depicted in Figure 5.4, exhibit a faint bluish-violet coloration. This coloration suggests the presence of the CH* radical, which emits chemiluminescence at a wavelength of 432 nm. It is observed that the luminosity of these images diminishes as the equivalence ratio decreases.

5.2.2 CH* chemiluminescence

CH* chemiluminescence refers to the emission of light from chemical reactions. The intensity of chemiluminescence radiation in combustion process is influenced by the chemical kinetics [52]. Reaction zone is identified using these characteristics.

In the non-premixed case of both PVRF and SPRF combustors, CH* radical concentration indicates reaction zone which is situated at the lower portion of the combustor. Intensity of this reaction zone decreases as the ϕ decreases. In premixed case, at higher ϕ the reaction zone is situated in the center of both PVRF and SPRF combustors. As ϕ decreases, reaction zone shifts towards the bottom of the combustor. This behavior is visible for both the combustors as the equivalence ratio ϕ decreases, intensity of CH* decreases (see Figure 5.5).

Figure 5.6 illustrates the spatial and temporal averaged intensity of CH* in the combustion process. In general, premixed cases exhibit higher CH* intensity compared to non-premixed cases. Specifically, in the non-premixed case, the PVRF combustor displays higher CH* intensity compared to the SPRF combustor. However, in the premixed cases, similar CH* intensities are observed between the two combustors. It is important to note that as the ϕ increases, the CH* intensity also increases in both combustors. This can be attributed to the higher temperatures associated with higher ϕ . Figure 5.6b shows the coefficient of variation of spatially averaged CH* intensity. The figure demonstrates that the fluctuation in total heat release is higher in the non-premixed case compared to premixed case. Fluctuations decreases as the global ϕ increases, for both the PVRF and SPRF combustors, SPRF combustor exhibits lower fluctuations in comparison to the PVRF combustor.

5.2 Experimental Results

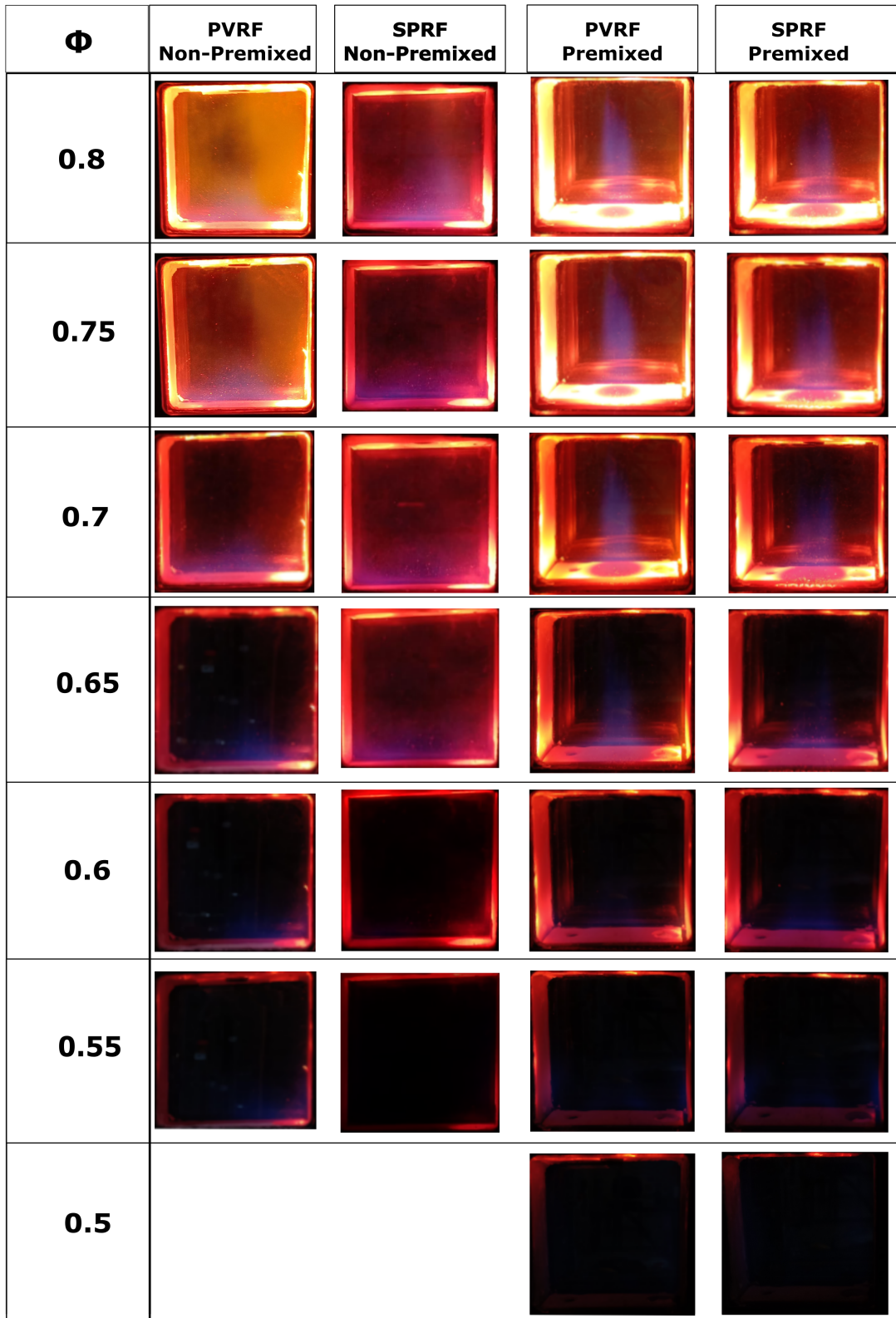


Figure 5.4: Global flame photographs of PVRF & SPRF combustor

5.2.3 Emissions characteristics

CO and NO_x emissions measurements (corrected to 15% of O_2 concentration) are presented in this section.

5.2 Experimental Results

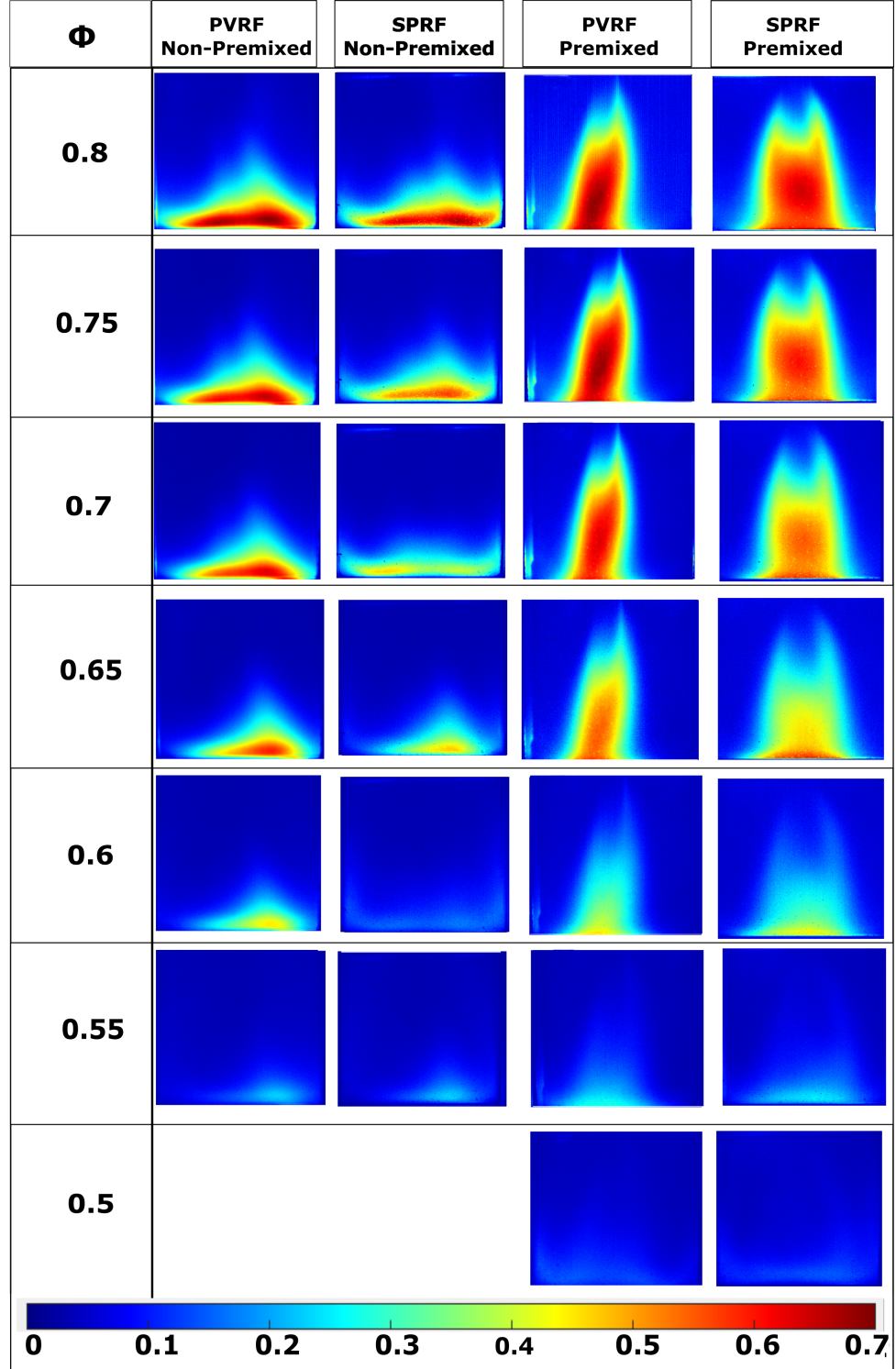


Figure 5.5: CH^* chemiluminescence intensity images.

CO Emissions

CO emissions are shown for all four cases in figure 5.7a. For non-premixed case, CO emissions are higher at high equivalence ratios and gradually decreases till $\phi = 0.7$ upto 32 ppm for PVRF and 24 for SPRF combustor, and then increases. From figure 5.7a it is clear that CO emissions

5.2 Experimental Results

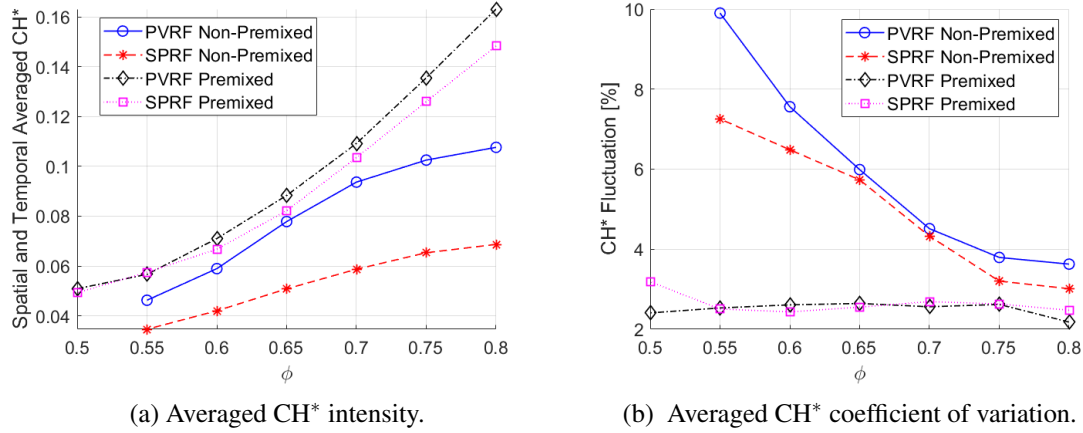


Figure 5.6: CH^* chemiluminescence data.

in SPRF combustor is lower than PVRF combustor for non-premixed case. For premixed case, CO emissions decreases upto $\phi = 0.55$ upto 21 ppm for PVRF and 13 ppm for SPRF combustor and then there is sudden jump in emission. Again CO emissions is lower in SPRF combustor than PVRF in premixed case. At lower equivalence ratios, the temperature field is reduced, leading to a lower conversion rate of CO to CO_2 . As a result, the levels of CO emissions increase in these conditions. One observation can be made that till $\phi = 0.65$ CO emissions are high in non-premixed case than premixed after that premixed case showed higher CO emissions than non-premixed case at higher equivalence ratios.

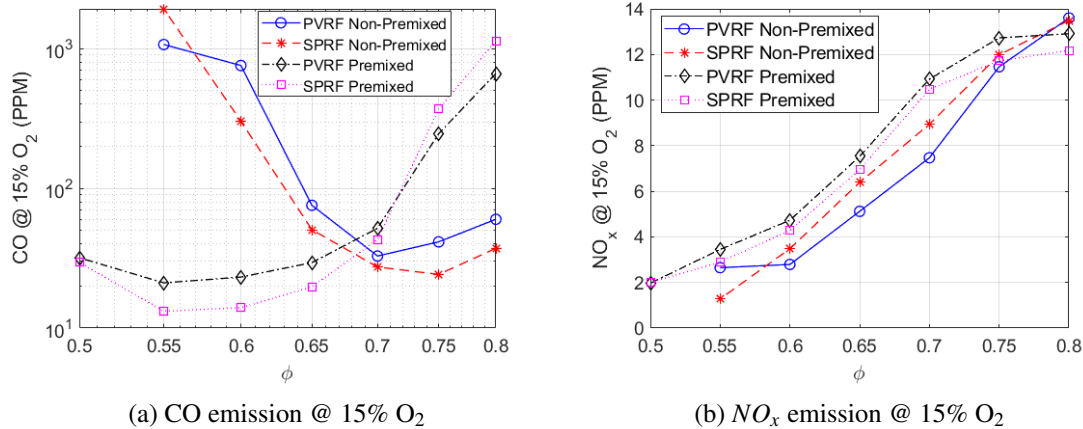


Figure 5.7: CO and NO_x Emissions.

NO_x Emissions

NO_x emissions are shown for all four cases in figure 5.7b. For all cases, the maximum NO_x emissions remain below 15 ppm when the equivalence ratio varies from 0.5 to 0.8 in the premixed case and 0.55 to 0.8 for non-premixed case. PVRF combustor in non-premixed case exhibits the

5.2 Experimental Results

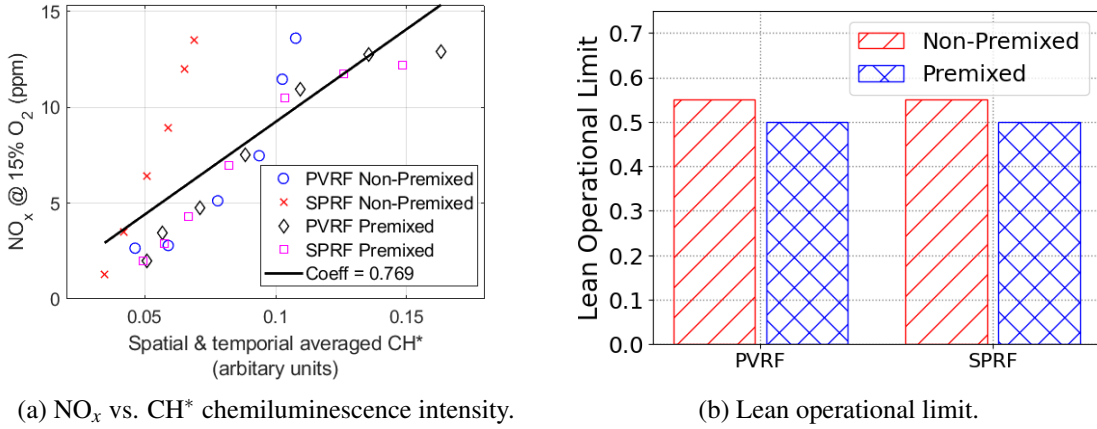


Figure 5.8: Nox vs. CH^* intensity and lean operational limit.

lowest NO_x emissions across the entire range of equivalence ratios. This is primarily attributed to the uniform and lower temperature distribution throughout the combustor, as well as improved fuel-oxidizer mixing. SPRF combustor shows higher NO_x emissions than PVRF combustor. These NO_x emissions are different from the generic NO_x distribution at high equivalence ratios due to high CO emissions.

NO_x and CH^* intensity

Figure 5.8a shows the correlation between NO_x emissions and the spatially and temporally averaged CH^* intensity. The graph illustrates a strong relationship between these two variables, particularly in the premixed case. It suggests that NO_x emissions can be effectively estimated using CH^* data, highlighting the potential for utilizing CH^* measurements as an indicator of NO_x emissions, especially in premixed mode.

Lean Operational Limit

Lean operational limit is determined by gradually decreasing the \dot{m}_{fuel} while keeping the \dot{m}_{air} constant until the flame extinguishes. The outcomes of this investigation are illustrated in Figure 5.8b. It can be observed that for both the PVRF and SPRF combustors, the lean limit is 0.5 for the premixed mode and 0.55 for the non-premixed mode.

CHAPTER 6

Conclusions and Future scope

6.1 Conclusions

In this work, two low emission reverse flow configurations are investigated through numerical and experimental analyses. In the numerical results, flow field characteristics, temperature field characteristics, and recirculation ratio within the combustors were investigated at a global equivalence ratio of 0.8 for non-reacting and reacting cases. The flow field and recirculation ratio results show better mixing in the PVRF combustor compared to the SPRF combustor. Temperature distribution is more uniform in SPRF combustor than PVRF combustor.

Experimental results, including global flame images and CH* chemiluminescence, revealed that in the non-premixed mode, the reaction initiated near the bottom of the combustor, while in the premixed mode, it occurred in the center. The non-premixed mode exhibited lower spatially and temporally averaged CH* intensity but higher fluctuations. Decreasing the equivalence ratio resulted in reduced combustion chamber intensity for both combustors. NOx emissions remained below 15 ppm, with the lowest emissions recorded as 1.3 ppm in the SPRF combustor for premixed mode at an equivalence ratio of 0.5, and 1.8 ppm in the PVRF combustor for non-premixed mode at an equivalence ratio of 0.6. The lowest CO emissions of 13 ppm and 21 ppm were measured for the SPRF and PVRF combustors, respectively, in the premixed mode at an equivalence ratio of 0.55. The obtained correlation between CH* intensity and NOx emissions suggests the potential for utilizing CH* measurements as an indicator of NOx emissions, especially in premixed mode.

6.2 Future scope

The current study was conducted on a small-scale combustor in the laboratory, operating at a maximum heat load of 6.25 kW. However, scaling practical combustors can be achieved by incorporating

6.2 Future scope

multiple fuel injection points. However, the presented approach still allows for the assessment of crucial practical factors such as pollutant emissions, pressure drop, combustion stability, and thermal intensity. By obtaining information on these parameters, we can gain a deeper understanding of the feasibility and performance of reverse flow combustors in real-world applications.

In future, experiments can be performed using Particle Image Velocimetry (PIV) and Planar Laser-Induced Fluorescence (PLIF). This will allow for a more comprehensive investigation of the flow field, which can then be used to validate the accuracy of the numerical results. Additionally, PLIF, can be employed to acquire detailed information about the intricate structure of the reaction zone, as well as the distribution of species and temperature. These techniques are particularly useful for studying turbulent combustion in both premixed and non-premixed modes. By utilizing PLIF, it becomes possible to identify regions of NO formation and explore innovative methods to minimize pollutant emissions.

Aircraft engines operate at even higher pressures, approximately 40 atm during takeoff and 10 atm during cruise. As a result, testing and exploring various pressure ranges can be beneficial for diverse applications in the field of gas turbine technology.

References

- [1] A. Gupta, Ashwani K., "Development of colorless distributed combustion for gas turbine application," Master's thesis, University of Maryland (College Park, Md.), 2011. [Online]. Available: <http://hdl.handle.net/1903/12230>
- [2] V. K. Arghode and A. K. Gupta, "Development of high intensity cdc combustor for gas turbine engines," *Applied Energy*, vol. 88, no. 3, pp. 963–973, 2011. [Online]. Available: <https://www.sciencedirect.com/science/article/pii/S0306261910003089>
- [3] A. H. Lefebvre and D. R. Ballal, *Gas turbine combustion*, 3rd ed. Boca Raton, FL: CRC Press, Jul. 2009.
- [4] Y. V. Lieuwen T.C., *Gas Turbine Emissions*. Cambridge University Press, 2013.
- [5] A. H. Lefebvre, *Gas Turbine Combustion: Alternative Fuels and Emissions*. CRC Press, 2010.
- [6] P. Sharma, N. Jain, and V. K. Arghode, "Investigation of a low emission liquid fueled reverse-cross-flow combustor," *Journal of Energy Resources Technology*, vol. 141, no. 10, p. 102202, 04 2019. [Online]. Available: <https://doi.org/10.1115/1.4043437>
- [7] A. K. Agarwal, A. P. Singh, and R. K. Maurya, "Evolution, challenges and path forward for low temperature combustion engines," *Progress in Energy and Combustion Science*, vol. 61, pp. 1–56, 2017. [Online]. Available: <https://www.sciencedirect.com/science/article/pii/S0360128516300739>
- [8] S. K. Gupta, "Investigation of a low emission reverse cross flow colorless combustor," Master's thesis, 2017. [Online]. Available: <http://172.28.64.70:8080/jspui/handle/123456789/16913>
- [9] C. Mendez, R. Parthasarathy, and S. Gollahalli, *Performance and Emission Characteristics of a Small-Scale Gas Turbine Engine Fueled with Ethanol/Jet A Blends*. [Online]. Available: <https://arc.aiaa.org/doi/abs/10.2514/6.2012-522>
- [10] R. N. Parthasarathy, S. Gollahalli, and C. Attaphong, *Combustion Properties of Jet A/Ethanol Blends in a Porous Media Burner*. [Online]. Available: <https://arc.aiaa.org/doi/abs/10.2514/6.2013-3677>
- [11] H. Cohen, G. Rogers, and H. Saravanamuttoo, *Gas turbine theory*. Longman Group Ltd, 1996.
- [12] J. Mattingly, *Elements of Gas Turbine Propulsion*, ser. AIAA education series. American Institute of Aeronautics and Astronautics, 2005. [Online]. Available: <https://books.google.co.in/books?id=vA98AAAACAAJ>
- [13] *Comparison of Liquid Fuel/Air Mixing and NOx Emissions for a Tangential Entry Nozzle*, ser. Turbo Expo: Power for Land, Sea, and Air, vol. Volume 3: Coal, Biomass and Alternative Fuels; Combustion and Fuels; Oil and Gas Applications; Cycle Innovations, 06 1994, v003T06A021. [Online]. Available: <https://doi.org/10.1115/94-GT-283>
- [14] T. Tanigawa, G.-M. Choi, K. Ebisui, S. Seno, and M. Kats. (1998) New combustion technology for low nitric oxides emission using highly preheated air. [Online]. Available: <https://collections.lib.utah.edu/ark:/87278/s6m61nt5>
- [15] R. Weber, A. K. Gupta, and S. Mochida, "High temperature air combustion (hitac): How it all started for applications in industrial furnaces and future prospects," *Applied Energy*, vol. 278, p. 115551, 2020. [Online]. Available: <https://www.sciencedirect.com/science/article/pii/S0306261920310631>
- [16] F. Weinberg, "Combustion temperatures: the future?" *Nature*, vol. 233, no. 5317, pp. 239–241, 1971.
- [17] A. K. Gupta, S. Bolz, and T. Hasegawa, "Effect of Air Preheat Temperature and Oxygen Concentration on Flame Structure and Emission," *Journal of Energy Resources Technology*, vol. 121, no. 3, pp. 209–216, 09 1999. [Online]. Available: <https://doi.org/10.1115/1.2795984>
- [18] H. Tsuji, A. K. Gupta, T. Hasegawa, M. Katsuki, K. Kishimoto, and M. Morita, *High temperature air combustion: from energy conservation to pollution reduction*, ser. Environmental & Energy Engineering. CRC Press, 2002.
- [19] M. MÖRTBERG, W. BLASIAK, and A. K. GUPTA, "Combustion of normal and low calorific fuels in high temperature and oxygen deficient environment," *Combustion Science and Technology*, vol. 178, no. 7, pp. 1345–1372, 2006. [Online]. Available: <https://doi.org/10.1080/00102200500325280>

-
- [20] A. K. Gupta, "Thermal Characteristics of Gaseous Fuel Flames Using High Temperature Air," *Journal of Engineering for Gas Turbines and Power*, vol. 126, no. 1, pp. 9–19, 03 2004. [Online]. Available: <https://doi.org/10.1115/1.1610009>
- [21] M. Mörtberg, W. Blasiak, and A. K. Gupta, "Experimental Investigation of Flow Phenomena of a Single Fuel Jet in Cross-Flow During Highly Preheated Air Combustion Conditions," *Journal of Engineering for Gas Turbines and Power*, vol. 129, no. 2, pp. 556–564, 05 2006. [Online]. Available: <https://doi.org/10.1115/1.2436558>
- [22] S. Lille, W. Blasiak, and M. Jewartowski, "Experimental study of the fuel jet combustion in high temperature and low oxygen content exhaust gases," *Energy*, vol. 30, no. 2, pp. 373–384, 2005, 3rd International Symposium on Advanced Energy Conversion Systems and Related Technologies. [Online]. Available: <https://www.sciencedirect.com/science/article/pii/S0360544204002725>
- [23] M. Mörtberg, "Study of gas fuel jet burning in low oxygen content and high temperature oxidizer," Ph.D. dissertation, KTH, Energy and Furnace Technology, 2005, qC 20100610.
- [24] W. Yang and W. Blasiak, "Chemical flame length and volume in liquified propane gas combustion using high-temperature and low-oxygen-concentration oxidizer," *Energy & Fuels*, vol. 18, no. 5, pp. 1329–1335, 2004. [Online]. Available: <https://doi.org/10.1021/ef0499168>
- [25] J. G. Wunning and J. A. Wunning, "Combustion chamber with flameless oxidation," Jun. 20 2006, uS Patent 7,062,917.
- [26] J. Wünning and J. Wünning, "Flameless oxidation to reduce thermal no-formation," *Progress in Energy and Combustion Science*, vol. 23, no. 1, pp. 81–94, 1997. [Online]. Available: <https://www.sciencedirect.com/science/article/pii/S0360128597000063>
- [27] W. Meier, M. Aigner *et al.*, "Flox® combustion at high pressure with different fuel compositions," in *ASME Turbo Expo 2007: Power for Land, Sea, and Air*. American Society of Mechanical Engineers Digital Collection, 2007, pp. 241–249.
- [28] A. Colorado, B. Herrera, and A. Amell, "Performance of a flameless combustion furnace using biogas and natural gas," *Bioresource Technology*, vol. 101, no. 7, pp. 2443–2449, 2010. [Online]. Available: <https://www.sciencedirect.com/science/article/pii/S0960852409015028>
- [29] O. Lammel, H. Schütz, G. Schmitz, R. Lückerath, M. Stöhr, B. Noll, M. Aigner, M. Hase, and W. Krebs, "FLOX® Combustion at High Power Density and High Flame Temperatures," *Journal of Engineering for Gas Turbines and Power*, vol. 132, no. 12, 08 2010, 121503. [Online]. Available: <https://doi.org/10.1115/1.4001825>
- [30] A. Cavaliere and M. de Joannon, "Mild combustion," *Progress in Energy and Combustion Science*, vol. 30, no. 4, pp. 329–366, 2004. [Online]. Available: <https://www.sciencedirect.com/science/article/pii/S0360128504000127>
- [31] G. Szegö, B. Dally, and G. Nathan, "Operational characteristics of a parallel jet mild combustion burner system," *Combustion and Flame*, vol. 156, no. 2, pp. 429–438, 2009. [Online]. Available: <https://www.sciencedirect.com/science/article/pii/S0010218008002551>
- [32] A. Cavigiolo, M. A. Galbiati, A. Effuggi, D. Gelosa, and R. Rota, "Mild combustion in a laboratory-scale apparatus," *Combustion Science and Technology*, vol. 175, no. 8, pp. 1347–1367, 2003. [Online]. Available: <https://doi.org/10.1080/00102200302356>
- [33] A. Effuggi, D. Gelosa, M. Derudi, and R. Rota, "Mild combustion of methane-derived fuel mixtures: Natural gas and biogas," *Combustion Science and Technology*, vol. 180, no. 3, pp. 481–493, 2008. [Online]. Available: <https://doi.org/10.1080/00102200701741368>
- [34] S. Kumar, P. Paul, and H. Mukunda, "Investigations of the scaling criteria for a mild combustion burner," *Proceedings of the Combustion Institute*, vol. 30, no. 2, pp. 2613–2621, 2005. [Online]. Available: <https://www.sciencedirect.com/science/article/pii/S0082078404000487>
- [35] R. Weber, J. P. Smart, and W. vd Kamp, "On the (mild) combustion of gaseous, liquid, and solid fuels in high temperature preheated air," *Proceedings of the Combustion Institute*, vol. 30, no. 2, pp. 2623–2629, 2005. [Online]. Available: <https://www.sciencedirect.com/science/article/pii/S0082078404001547>
- [36] B. Dally, E. Riesmeier, and N. Peters, "Effect of fuel mixture on moderate and intense low oxygen dilution combustion," *Combustion and Flame*, vol. 137, no. 4, pp. 418–431, 2004. [Online]. Available: <https://www.sciencedirect.com/science/article/pii/S0010218004000574>
- [37] V. K. Arghode and A. K. Gupta, "Investigation of forward flow distributed combustion for gas turbine application," *Applied Energy*, vol. 88, no. 1, pp. 29–40, 2011. [Online]. Available: <https://www.sciencedirect.com/science/article/pii/S0306261910001376>
- [38] V. K. Arghode, A. K. Gupta, and K. M. Bryden, "High intensity colorless distributed combustion for ultra low emissions and enhanced performance," *Applied Energy*, vol. 92, pp. 822–830, 2012. [Online]. Available: <https://www.sciencedirect.com/science/article/pii/S0306261911005496>
- [39] V. K. Arghode and A. K. Gupta, "Role of thermal intensity on operational characteristics of ultra-low emission colorless distributed combustion," *Applied Energy*, vol. 111, pp. 930–956, 2013. [Online]. Available: <https://www.sciencedirect.com/science/article/pii/S0306261913005461>

-
- [40] ——, “Hydrogen addition effects on methane–air colorless distributed combustion flames,” *International Journal of Hydrogen Energy*, vol. 36, no. 10, pp. 6292–6302, 2011. [Online]. Available: <https://www.sciencedirect.com/science/article/pii/S0360319911003454>
- [41] ——, “Effect of flow field for colorless distributed combustion (cdc) for gas turbine combustion,” *Applied Energy*, vol. 87, no. 5, pp. 1631–1640, 2010. [Online]. Available: <https://www.sciencedirect.com/science/article/pii/S0306261909004243>
- [42] ——, “Investigation of reverse flow distributed combustion for gas turbine application,” *Applied Energy*, vol. 88, no. 4, pp. 1096–1104, 2011. [Online]. Available: <https://www.sciencedirect.com/science/article/pii/S0306261910004411>
- [43] Y. He, “Flameless combustion of natural gas in the sj/wj furnace,” 2008, p. 213. [Online]. Available: <https://www.semanticscholar.org/paper/Flameless-Combustion-of-Natural-Gas-in-the-SJ-WJ-He/1935bd24ea8eab4534b01b33e39ff6ea1762cdb7>
- [44] A. Sobiesiak, S. Rahbar, and H. A. Becker, “Performance characteristics of the novel low-nox cgri burner for use with high air preheat,” *Combustion and Flame*, vol. 115, no. 1, pp. 93–125, 1998. [Online]. Available: <https://www.sciencedirect.com/science/article/pii/S0010218097003660>
- [45] D. Rhode, D. Lilley, and D. McLaughlin, “Mean flowfields in axisymmetric geometries with swirl combustor,” *AIAA Journal*, vol. 21, no. 4, pp. 593–600, 1983. [Online]. Available: <https://doi.org/10.2514/3.60127>
- [46] R. A. Yetter, I. Glassman, and H. C. Gabler, “Asymmetric whirl combustion: A new low nox approach,” *Proceedings of the Combustion Institute*, vol. 28, no. 1, pp. 1265–1272, 2000. [Online]. Available: <https://www.sciencedirect.com/science/article/pii/S0082078400803392>
- [47] S. Kumar, P. Paul, and H. Mukunda, “Studies on a new high-intensity low-emission burner,” *Proceedings of the Combustion Institute*, vol. 29, no. 1, pp. 1131–1137, 2002, proceedings of the Combustion Institute. [Online]. Available: <https://www.sciencedirect.com/science/article/pii/S1540748902801432>
- [48] T. Rutar, P. C. Malte, and J. C. Kramlich, “Investigation of nox and co formation in lean-premixed, methane/air, high-intensity, confined flames at elevated pressures,” *Proceedings of the Combustion Institute*, vol. 28, no. 2, pp. 2435–2441, 2000. [Online]. Available: <https://www.sciencedirect.com/science/article/pii/S0082078400806578>
- [49] K.-Y. Hsu, L. P. Goss, and W. M. Roquemore, “Characteristics of a trapped-vortex combustor,” *Journal of Propulsion and Power*, vol. 14, no. 1, pp. 57–65, 1998. [Online]. Available: <https://doi.org/10.2514/2.5266>
- [50] C. L. Vandervort, “9 ppm NOx/CO Combustion System for “F” Class Industrial Gas Turbines ,” *Journal of Engineering for Gas Turbines and Power*, vol. 123, no. 2, pp. 317–321, 01 2001. [Online]. Available: <https://doi.org/10.1115/1.1362661>
- [51] K. Ahmad and V. K. Arghode, “Experimental investigation of a jet-a1 fuelled peripheral vortex reverse flow combustor,” *Thermal Science and Engineering Progress*, vol. 21, p. 100754, 2021. [Online]. Available: <https://www.sciencedirect.com/science/article/pii/S2451904920302742>
- [52] K. Ahmad, S. K. Gupta, and V. K. Arghode, “Investigation of a low emission peripheral vortex reverse flow (pvrf) combustor fuelled by lpg and ethylene,” *Journal of the Energy Institute*, vol. 108, p. 101200, 2023. [Online]. Available: <https://www.sciencedirect.com/science/article/pii/S1743967123000296>
- [53] S. K. Gupta, A. K. Kushwaha, and V. K. Arghode, “Investigation of peripheral vortex reverse flow (pvrf) combustor for gas turbine engines,” *Energy*, vol. 193, p. 116766, 2020. [Online]. Available: <https://www.sciencedirect.com/science/article/pii/S0360544219324612>
- [54] R. Sood, P. Sharma, and V. K. Arghode, “Combustion Characteristics of a Peripheral Vortex Reverse Flow Combustor With Coaxial Fuel Injection,” *Journal of Energy Resources Technology*, vol. 142, no. 5, 02 2020, 052302. [Online]. Available: <https://doi.org/10.1115/1.4046386>
- [55] M. K. Bobba, P. Gopalakrishnan, J. Seitzman, and B. Zinn, “Characteristics of combustion processes in a stagnation point reverse flow combustor,” in *Turbo Expo: Power for Land, Sea, and Air*, vol. 42363, 2006, pp. 867–875.
- [56] M. K. Bobba, P. Gopalakrishnan, K. Periagaram, and J. M. Seitzman, “Flame Structure and Stabilization Mechanisms in a Stagnation-Point Reverse-Flow Combustor,” *Journal of Engineering for Gas Turbines and Power*, vol. 130, no. 3, 04 2008, 031505. [Online]. Available: <https://doi.org/10.1115/1.2836614>
- [57] *Stagnation-Point Reverse-Flow Combustor Performance With Liquid Fuel Injection*, ser. Turbo Expo: Power for Land, Sea, and Air, vol. Volume 1: Combustion and Fuels, Education, 05 2006. [Online]. Available: <https://doi.org/10.1115/GT2006-91338>
- [58] P. Gopalakrishnan, P. Alison, and J. Seitzman, “Effects of fuel injection and mixing on nox performance of a liquid-fueled stagnation point reverse flow combustor,” in *5th US Combustion Meeting, University of California at San Diego, CA, Mar*, 2007, pp. 25–28.
- [59] C. Duwig and P. Iudiciani, “Large eddy simulation of turbulent combustion in a stagnation point reverse flow combustor using detailed chemistry,” *Fuel*, vol. 123, pp. 256–273, 2014. [Online]. Available: <https://www.sciencedirect.com/science/article/pii/S001623611400088X>

-
- [60] P. Li, F. Wang, J. Mi, B. B. Dally, and Z. Mei, "Mild combustion under different premixing patterns and characteristics of the reaction regime," *Energy & Fuels*, vol. 28, no. 3, pp. 2211–2226, 2014. [Online]. Available: <https://doi.org/10.1021/ef402357t>
- [61] M. A. Nemitalah, S. S. Rashwan, I. B. Mansir, A. A. Abdelhafez, and M. A. Habib, "Review of novel combustion techniques for clean power production in gas turbines," *Energy & Fuels*, vol. 32, no. 2, pp. 979–1004, 2018. [Online]. Available: <https://doi.org/10.1021/acs.energyfuels.7b03607>
- [62] S. R. Turns, *An Introduction To Combustion: Concepts And Applications*. McGraw-Hill Education, 2011.
- [63] L. Forney and N. Nafia, "Turbulent jet reactors: Mixing time scales," *Chemical Engineering Research and Design*, vol. 76, no. 6, pp. 728–736, 1998, process Design. [Online]. Available: <https://www.sciencedirect.com/science/article/pii/S0263876298717034>
- [64] H. J. Hussein, S. P. Capp, and W. K. George, "Velocity measurements in a high-reynolds-number, momentum-conserving, axisymmetric, turbulent jet," *Journal of Fluid Mechanics*, vol. 258, p. 31–75, 1994.
- [65] F. P. Ricou and D. B. Spalding, "Measurements of entrainment by axisymmetrical turbulent jets," *Journal of Fluid Mechanics*, vol. 11, no. 1, p. 21–32, 1961.
- [66] V. N. Nori and J. M. Seitzman, "Ch chemiluminescence modeling for combustion diagnostics," *Proceedings of the Combustion Institute*, vol. 32, no. 1, pp. 895–903, 2009. [Online]. Available: <https://www.sciencedirect.com/science/article/pii/S1540748908001089>
- [67] F. V. Tinaut, M. Reyes, B. Giménez, and J. V. Pastor, "Measurements of oh and ch chemiluminescence in premixed flames in a constant volume combustion bomb under autoignition conditions," *Energy & Fuels*, vol. 25, no. 1, pp. 119–129, 2011. [Online]. Available: <https://doi.org/10.1021/ef1013456>
- [68] S. Karnani and D. Dunn-Rankin, "Visualizing ch* chemiluminescence in sooting flames," *Combustion and Flame*, vol. 160, no. 10, pp. 2275–2278, 2013. [Online]. Available: <https://www.sciencedirect.com/science/article/pii/S0010218013001752>